R. & M. No. 2895
(13,322, 14,608)
A.R.C. Technical Report

MINISTRY OF SUPPLY

AERONAUTICAL RESEARCH COUNCIL
REPORTS AND MEMORANDA

Rolling Power Measurements and Comparative Calculations for a Flexible Model Wing Constructed from Xylonite

By

N. C. LAMBOURNE, A. S. BATSON and A. CHINNECK,
of the Aerodynamics Division, N.P.L.

With an Appendix by H. C. GARNER,
of the Aerodynamics Division, N.P.L.

LONDON : HER MAJESTY'S STATIONERY OFFICE
1955
PRICE 9*s* 6*d* NET

Rolling Power Measurements and Comparative Calculations for a Flexible Model Wing Constructed from Xylonite

By

N. C. LAMBOURNE, A. S. BATSON and A. CHINNECK,
of the Aerodynamics Division, N.P.L.

With an Appendix by H. C. GARNER,
of the Aerodynamics Division, N.P.L.

Reports and Memoranda No. 2895*

February, 1952

Summary.—Partly to gain experience of aero-elastic models constructed from Xylonite, and partly to provide information regarding loss of rolling power due to wing distortion, a tip-to-tip model of the wings of a *Spitfire* aircraft was constructed. It was mounted on a longitudinal axis in a wind tunnel so that it could roll continuously. Rates of rolling were measured for a range of air speeds and the results are compared with those of calculations.

The variation of rolling power with air speed was calculated by :

(*a*) the Collar and Broadbent method (R. & M. 2186) which is based on strip theory,

(*b*) a method developed by H. C. Garner based on lifting-line theory.

If the aerodynamic quantity $a_2/a_1 m$ is assumed to take its two-dimensional theoretical value, the Collar and Broadbent method yields a good estimate of the ratio of the rolling power at any speed to the ' rigid-wing ' rolling power, and thus successfully predicts the reversal speed. The Garner lifting-line method gives a reversal speed which is high in comparison with experiment. The estimated rolling power is proportional to the two-dimensional value of a_2/a_1 which is uncertain within $\pm$ 5 per cent. The measured rolling power is somewhat less than that estimated by either method, but this discrepancy may be due to the waviness over the surface of the model.

The results of calculations of the reversal speed by two early and more approximate methods (R. & M. 1568 and 2059) are also included. These give values below that indicated by the experiment.

Concerning the use of Xylonite models for aero-elastic work, it is concluded that the lower limit which must be placed on the thickness of the skin of the model to provide a reasonable aerodynamic surface, will tend to produce models too stiff to be capable of adequately showing up aero-elastic effects in a low-speed tunnel. It is suggested that Xylonite aero-elastic models will find their greatest use at high speeds. It is also concluded that in constructing a Xylonite replica model of a full-scale structure particular care must be taken to ensure that the stiffnesses are correctly represented.

1. *Introduction.*—The following experiments were undertaken with the dual purpose of gaining experience of Xylonite† models for aero-elastic research, and of providing an experimental comparison with calculations of loss of rolling power due to wing twist. Redshaw, having used with success Xylonite models for structural research[1], suggested that this material might be suitable for constructing scale models for flutter tests[2], and some assessment of its capabilities in this direction was required. About the same time as this suggestion was made, there was a call for experimental work in connection with aileron reversal and this led to the instigation of the present tests by the Oscillation Sub-Committee of the Aeronautical Research Council.

* Published with the permission of the Director, National Physical Laboratory.

† Xylonite—trade name for cellulose nitrate manufactured by BX Plastics.

As a test of the Xylonite model technique it was decided to construct a scale model of the wings of a particular type of aeroplane. A consideration of the size of the available wind tunnel and the possible scale factors that could be attained, suggested that a model of the *Spitfire* V would be most convenient. In addition the plan-form of the wings of this aircraft had a large variation of aileron chord ratio over the span, which made it a difficult subject to treat by the earlier and more approximate methods of reversal speed calculation[3], and therefore a good test for a more exact method[4].

The model consisted of a tip-to-tip unit mounted on an axis running through a dummy fuselage so that it was free to roll continuously. Rates of rolling due to aileron deflection were measured for a range of air speeds. Calculations of rolling power and aileron reversal speed were made by several methods, and the results are compared with the measurements.

2. *Main Symbols and General Data.*—The system of axes and sign convention are shown in Fig. 3.

b		Total span (tip-to-tip) = 5·293 ft
s		Semi span (centre-line to tip) = 2·649 ft
c_m		Mean chord = 0·928 ft
S		Gross wing area = 4·919 sq ft
η		Spanwise co-ordinate, y/s
ϕ		Angle of bank in tunnel (*see* Fig. 3)
ξ		Aileron angle (*see* Fig. 3), ξ_0 refers to station $\eta = 0{\cdot}57$
θ		Angle of wing twist (*see* Fig. 3), θ_0 refers to station $\eta = 0{\cdot}57$
ψ'		Wing distortion (*see* Fig. 16)
ψ''		Wing distortion (*see* Fig. 16), ψ''_0 refers to station $\eta = 0{\cdot}57$
m_θ		Torsional stiffness
C_l		Rolling-moment coefficient due to ailerons = $L/\frac{1}{2}\rho V^2 bS$
l_p		Rolling-moment derivative due to rolling = $4L_p/\rho V b^2 S$
p		Angular velocity of rolling
V_r		Air speed for aileron reversal
a_1	=	$\partial C_L/\partial\theta$ appropriate to strips
a_2	=	$\partial C_L/\partial\xi$ appropriate to strips
$(a_2/a_1)_0$		Value of (a_2/a_1) at station $\eta = 0{\cdot}57$
m	=	$-\partial C_m/\partial\xi$ (at constant C_L) appropriate to strips
$(ps/\xi_0 V)$		Rolling power
$(ps/\xi_0 V)_0$		' Rigid-wing ' rolling power corresponding to a geometrically similar but rigid wing, assumed to be identical with ' initial ' rolling power for condition $V \to 0$
		Aileron extent $0{\cdot}497 < \eta < 0{\cdot}872$
		Wing root at $\eta = 0{\cdot}079$
		Mean aileron-to-wing chord ratio $E = 0{\cdot}17$ (aileron chord measured from hinge-line to trailing edge)
		Overall linear scale of model 1/7
		Material thickness scale (nominal) 1·3/7

3. *General Description of Model.*—The complete model consisted of two separate Xylonite wings attached to a wooden ' fuselage ' as shown in the photograph (Fig. 1). The fuselage was a solid of revolution comprising two principal parts—the forward part to which the wings were attached, and the rear portion which carried two ball-bearings forming an axis of roll for the combination of the front part and the wings. The general arrangement of the shaft and bearings is shown diagrammatically in Fig. 4. The bearings themselves were carefully chosen from stock for low friction. The method of supporting the model in the National Physical Laboratory 9-ft $\times$ 7-ft wind tunnel is shown by Figs. 2 and 5. The rear portion of the fuselage was supported centrally in the tunnel by 4 streamlined struts at its forward end and a cone of bracing wires at its tail end. The final adjustments of the position of the model in the tunnel involved an approximate measurement of the lift developed at a number of angular positions of the wings, and for this purpose the upper vertical supporting strut was attached to the tunnel structure by an electrical resistance strain-gauge ring ; the lower vertical strut could be either locked to the tunnel structure or, during the measurement of lift, left unconstrained in the vertical direction but tensioned with an adequate load. The horizontal struts were attached to the tunnel in a similar manner.

The wings and fuselage combination was carefully balanced about the axis of roll. During the rolling-speed tests the wings were free to rotate continuously, whilst for the measurement of rolling moments a lever arm could be rigidly attached to the main shaft and connected to a balance above the roof of the tunnel. It was possible to measure the rolling moment at a number of angles of bank.

4. *The Wings.*—The model was intended to reproduce the elastic characteristics of the *Spitfire* wing, and major structural components were Xylonite replicas of their full-scale counterparts reduced to an overall linear scale of 1/7, but the sheet thicknesses were relatively greater. The construction was carried out by Messrs. Boulton Paul working to the basic drawings of the *Spitfire* V. Figs. 6 and 7 show the general structural layout of a wing. The torsion resisting component consisted of a D nose box ; the skin between the main spar and the rear spar had numerous ' cut-outs ' and was thin in comparison with that over the D nose. The main departure from Xylonite was the construction of the aileron and the wing tip (*i.e.*, the portion of the wing outboard of the aileron) from mahogany, drilled and covered with Xylonite for lightness. Both these model components could be regarded as rigid. For simplicity the ribs were of sheet construction, 0·010-in. thick, as against the lattice girder type of construction of full-scale.

For the attachment of the wings to the fuselage, the main spar of each wing carried a steel shaft which could be firmly clamped in a housing on the fuselage. Independent incidence adjustment of each wing was possible by unclamping and rotating the wing on its shaft. A single point location was provided at the root of the rear spar. This method of supporting the wings on the fuselage was considered to be representative of full-scale.

Each aileron was attached to its wing by hinges at two positions along its span, and it could be set at an angle by a clamping device situated at a position $\eta = 0{\cdot}57$, corresponding approximately to that of the full-scale control.

5. *Scale Factors.*—If Reynolds number effects are neglected, dynamical similarity between model and full-scale is achieved for static aero-elastic effects when the parameter $C/\rho V^2 L^3$ is the same for both model and full-scale, C being a typical angular elastic stiffness and L a typical external dimension. Now the stiffness scale for externally similar structures built of sheet materials for which the thicknesses t are small in comparison with the other dimensions[2] is

$$C_M/C_F = (E_M/E_F)(t_M/t_F)(L_M/L_F)^2 = k(E_M/E_F)(L_M/L_F)^3$$

where $k(L_M/L_F) = t_M/t_F$, E is Young's modulus, and $_M$ and $_F$ refer to model and full-scale respectively.

The speed scale for aero-elastic effects is then given by

$$(V_M/V_F)^2 = (\rho_F/\rho_M)(L_F/L_M)^3(C_M/C_F) = k(\rho_F/\rho_M)(E_M/E_F).$$

When $\rho_F/\rho_M = 1$,

$E_M = 0{\cdot}31 \times 10^6$ lb/in.^{2} (Xylonite),

and $E_F = 10 \times 10^6$ lb/in.^{2} (Dural),

then $(V_M/V_F)^2 = 0{\cdot}031k$

Since the aileron reversal speed for the *Spitfire* is in the neighbourhood of 900 ft/sec it was convenient to design for a speed scale of 1/5 which would correspond to a model reversal speed of approximately 180 ft/sec ; this led to a nominal design value $k = 1{\cdot}3$.

The Xylonite sheets used in the construction were of normal stock thicknesses and the following table compares the full-scale and model thicknesses of the main components.

Component	Full-scale t_F (in.)	Model t_M (in.)	$k = 7 \times \frac{t_M}{t_F}$	$k/1{\cdot}3$
Root portion of main spar web	12G, 0·104	0·020	1·35	1·04
Tip portion of main spar web	16G, 0·064	0·010	1·09	0·84
Skin of D nose	14G, 0·080	0·015	1·31	1·01
Remainder of skin (*i.e.*, aft of main spar) ..	24G, 0·022	0·0075	2·38	1·83

It was understood that the rear portion of the *Spitfire* skin was almost completely ineffective in providing torsional stiffness owing to the large number of cut-outs. True scaling down of the thickness of this portion using the nominal factor $k = 1{\cdot}3$ would have required a model thickness of 0·004 in. This thickness was regarded as unworkable, and the skin was constructed from 0·0075-in. sheet, since it was thought that, provided the cut-outs were correctly reproduced on the model, the extra thickness would have no effect on the design torsional stiffness. However, the model proved to be considerably stiffer than expected, but this question is dealt with in section 7.

From the aerodynamic point of view, the surface of the wing behind the main spar was bad owing to its waviness. The surface of the D nose was quite good, which suggests that if the whole surface could have been constructed with a similar thickness (*i.e.*, 0·015 in.) or possibly even 0·010 in. a satisfactory aerodynamic surface would have been achieved. This is an example of what is probably the principal difficulty in designing Xylonite replica models for static aeroelastic or flutter tests. Stated fairly generally, it is that to obtain a speed scale which will allow the range of full-scale speeds to be covered by tests in a normal low-speed tunnel (say one having a 9-ft × 7-ft working-section and a maximum speed of 230 ft/sec) the required skin thicknesses will probably be insufficient to provide a good aerodynamic surface, and may even prove to be so small as to be unworkable.

6. *Stiffness Tests.*—The twists at a number of spanwise stations along each wing were measured for a couple applied just inboard of the rigid wing tip (*i.e.*, Rib 21, $\eta = 0{\cdot}87$). The wing was supported in a manner that simulated its attachment to the fuselage, and couples were applied by a wooden template fitting over the profile ; angles of twist were measured by two small concave mirrors fixed by Plasticene to the undersurface of the wing at the main spar position, one at a variable station, the other at a master station at Rib 20 ($\eta = 0{\cdot}83$). Distortion modes $F_s(\eta)$ were obtained as the ratios of the twists at the variable, to those at the master station. Routine stiffness checks were made by measuring twists at the master station only.

Flexural centre positions were obtained at 3 spanwise stations $\eta = 0{\cdot}42$, $0{\cdot}66$ and $0{\cdot}87$. For each of these measurements the particular section was loaded at a number of chordwise positions and the twist at the section measured in each case. The chordwise position of the load for which the twist was zero, the flexural centre, was then found by interpolation.

Some creep occurred immediately after a load had been applied to the wing and Fig. 8 shows the results of two typical creep tests in which the wing was loaded with a couple of approximately half the maximum value used during the stiffness measurements. It will be noticed that the twist did eventually return to zero after the load had been removed, and that the path of the return after unloading was similar in nature to the path after loading. From the point of view of creep, the wings were considered to be comparable with flutter models consisting of a wooden framework covered with silk.

The stiffness as measured at the master station showed an unaccountable daily variation. Readings of atmospheric temperature and humidity were taken for each stiffness test, since it appeared that these factors had an appreciable effect on the elastic properties of cellulose nitrate[5], but in a total of 22 daily stiffness measurements no correlation was apparent. One possible explanation based on the fact that the elastic modulus of Xylonite depends on the water content, is that the water content takes some time to reach its equilibrium level after a change of humidity, and thus that the stiffness would not depend only on the current humidity, but on its previous time history. In 16 measurements of stiffness on the port wing the maximum variations were + 9 per cent and — 12 per cent of the mean, and in 20 measurements on the starboard wing similar variations were + 6 per cent and — 5 per cent.

The mean values of the stiffnesses measured at $\eta = 0{\cdot}83$ were

Port	65 lb ft/radn
Starboard	61 ,, ,,
Mean	63 ,, ,,

The measured modes of static distortion are shown in Fig. 9.

During the stiffness tests the maximum twist allowed at $\eta = 0{\cdot}83$ was approximately $0{\cdot}7$ deg, the linearity of deflection with load was excellent up to this angle of twist at least.

The positions of the flexural centre in local chords aft of the leading edge were:

	$\eta = 0{\cdot}42$	$0{\cdot}66$	$0{\cdot}87$
Port	$0{\cdot}19$	$0{\cdot}20$	$0{\cdot}16$
Starboard	$0{\cdot}28$	$0{\cdot}18$	$0{\cdot}29$

7. *Comparison between Measured and Predicted Stiffnesses.*—The theoretical ratio of the model to the full-scale stiffness is

$$C_M/C_F = k(E_M/E_F)(L_M/L_F)^3$$
$$= 1{\cdot}17_5 \times 10^{-4}$$

when the following design values are inserted:

$$k = 1{\cdot}3$$
$$E_M/E_F = 0{\cdot}31/10$$
$$L_M/L_F = 1/7.$$

The following table compares the measured model and full-scale torsional stiffnesses at a few spanwise positions, the full-scale values having been supplied by the Royal Aircraft Establishment. Both full-scale and model measurements were made by applying a couple near the wing tip.

Full-scale		Model			$(m_\theta)_M/(m_\theta)_F$
Spanwise station. Distance from centre-line	$(m_\theta)_F$	Equivalent station. Distance from centre-line	$F_s(\eta)$ interpolated from Fig. 9	$(m_\theta)_M = 63/F_s(\eta)$	
(in.)	lb ft/radn	(in.)		lb ft/radn	
79	11×10^5	11·3	0·17	370	$3{\cdot}4 \times 10^{-4}$
147	$4{\cdot}9 \times 10^5$	21·0	0·53	120	$2{\cdot}5 \times 10^{-4}$
192	$1{\cdot}65 \times 10^5$	27·4	1·15	55	$3{\cdot}3 \times 10^{-4}$
					Mean $= 3{\cdot}1 \times 10^{-4}$

From the theoretical value of C_M/C_F and the quoted full-scale stiffnesses, an estimate gives the model torsional stiffness at $\eta = 0{\cdot}83$ as 24 lb ft/radn in comparison with the measured value of 63 lb ft/radn. The model torsional stiffness that was realised is thus approximately 2·6 times that which is predicted from the design scale factors. This large discrepancy cannot be completely accounted for by the fact that the thickness of the rear skin of the model was greater than the correctly scaled down value, for even in the hypothetical case in which all the components are correspondingly thickened the theoretical value of $(m_\theta)_M/(m_\theta)_F$ is only $2{\cdot}1 \times 10^{-4}$.

There is much better agreement between the flexural stiffnesses, the ratio $(l_\phi)_M/(l_\phi)_F$ being $1{\cdot}48 \times 10^{-4}$.

Although the discrepancy with regard to the torsional stiffness cannot be completely explained, it is probable that the cut-outs in the wing were not adequately reproduced and that, in comparison with full-scale, the rear skin was too firmly attached to the main spar. On the completion of the first series of wind-tunnel tests, the structure of the model wings was altered in an attempt to reduce the torsional stiffness ; this is dealt with later in section 11.

8. *Alignment of Model in Wind Tunnel.*—Before carrying out the rolling speed tests it was necessary to align the rolling axis of the model along the effective wind axis of the tunnel. In addition, to prevent any possible overstressing of the wings, the effective incidence of each was adjusted to approximately zero. These two types of adjustment were effected concurrently by a trial-and-error method involving the measurement of rolling moment and lift (*i.e.*, normal force) for angles of bank 0 deg, 90 deg, 180 deg, and 270 deg. The normal force was not measured accurately, but an indication of whether the model was developing lift was obtained from the appropriate strain gauge unit. No single alignment of the rolling axis and incidence setting of the wings could satisfy the condition of zero lift, and zero rolling moment at all 4 orientations of the model, and a compromise had to be made. Later some investigation of the variation of rolling moment with angle of bank was made and this is dealt with in section 10.

9. *Rolling Speed Tests.*—The port and starboard ailerons were given an equal but opposite setting and the time for a number (usually 10) of complete revolutions was obtained with a stopwatch for a range of air speeds. The measurements covered the range of aileron angles $\xi_0 = \pm 4$ deg, $\pm$ 6 deg, $\pm$ 8 deg and $\pm$ 10 deg for speeds up to 190 ft/sec. The tunnel was actually capable

of running up to 220 ft/sec, but there seemed to be no particular value in extending the tests up to this speed, especially since the model was likely to be damaged by the particles of tunnel dust which were carried by the air at these higher speeds.

For a combination of small aileron angle and low air speed the rolling motion of the model was erratic, due presumably to non-uniformities in the stream, but for aileron angles above 2 deg and air speeds above 20 ft/sec the motion appeared to be quite steady. The possible effect of the non-uniformities of the stream on the rolling speeds is dealt with in section 10. To test whether the struts which supported the model had any effect on the rolling speed, 4 dummy struts were placed in the diagonal positions, so that, in all, there were 8 equally spaced struts around the axis. A number of rolling speed tests were repeated, and since the addition of the dummy struts produced a negligible change in rolling speed, it was concluded that the interference due to the supporting struts was not serious.

Rates of rotation were plotted against aileron angle for each wind speed and were found to be reasonably linear as shown in Fig. 10. The slopes p/ξ_0 were obtained and these together with the non-dimensional parameter $(ps/\xi_0 V)$ are plotted in Fig. 11, to show the variation of rolling power with air speed. The figure also includes some of the calculated results to be referred to later.

Simple theory[7] gives the relation between the steady rate of rolling and the air speed as:

$$p/\xi_0 V = k(1 - V^2/V_r^2) \quad .. \quad .. \quad .. \quad .. \quad .. \quad .. \quad .. \quad (1)$$

or

$$p/\xi_0 V^3 = k(1/V^2 - 1/V_r^2) \quad .. \quad .. \quad .. \quad .. \quad .. \quad .. \quad .. \quad (2)$$

where k is a constant involving the aerodynamic properties of the system and V_r is the reversal speed, which involves both the aerodynamic and the elastic properties.

As suggested by Victory[3] equation (2) may be used to give a linear plot between $p/\xi_0 V^3$ and $1/V^2$ from which $1/V_r^2$, and thus V_r, may be obtained by extrapolation. Fig. 12 shows the experimental results plotted in this way and leads to an extrapolated reversal speed of 309 ft/sec.

10. *Variation of Rolling Moment with Angle of Bank.*—During measurements of l_p using the free rolling of a model in a wind tunnel Evans and Fink[6] found a variation of rolling moment with angle of bank which they attributed to secondary flow in the tunnel stream. To take account of this phenomenon these authors developed corrections to be applied to the measured rates of rolling as follows.

The rolling moment is written in the form $C_l + C_l(\phi)$, where the first term refers to the net contribution due to aileron displacement and wing distortion, and the second term to the variation of rolling moment due to angle of bank ϕ. The equation of motion of the system is then

$$A\frac{d^2\phi}{dt^2} - \tfrac{1}{4}\rho SVb^2 l_p \frac{d\phi}{dt} = \tfrac{1}{2}\rho V^2 Sb[C_l + C_l(\phi)] \quad .. \quad .. \quad .. \quad (3)$$

where A is the moment of inertia about the rolling axis and the other symbols have their usual significance.

The variation of rolling moment with position may be written in the form

$$C_l(\phi) = \sum_1^n (A_n \sin n\phi + B_n \cos n\phi) . \quad .. \quad .. \quad .. \quad .. \quad .. \quad .. \quad (4)$$

Solution of equation (3) leads to the conclusion that the observed periodic time T is in excess of the periodic time T_0 corresponding to a similar system but with $C_l(\phi) = 0$ in which case the period is given simply as

$$T_0 = \frac{\pi b}{V}\frac{l_p}{C_l} . \quad .. \quad .. \quad .. \quad .. \quad .. \quad .. \quad .. \quad .. \quad .. \quad (5)$$

The relation between T and T_0 is expressible in the form

$$T = T_0(1 + \varepsilon)$$

or

$$T = T_0(1 + \delta_1 h + \delta_2 h^2 + \delta_3 h^3 + \text{etc.}) \quad .. \quad .. \quad .. \quad .. \quad .. \quad (6)$$

where both h and δ are small quantities.

It may be shown that

$$\delta_1 = 0$$

$$\delta_2 h^2 = \sum_1^n \frac{(A_n^2 + B_n^2)}{2C_l^2(1 + 64n^2C_l^2A^2/\rho^2S^2b^6l_p^4)}$$

and that the subsequent terms in equation (6) are all small in comparison with $\delta_2 h^2$.

Values of $C_l(\phi)$ measured at 60 and 100 ft/sec are shown plotted in Fig. 13 together with a 'least-squares' curve

$$C_l = \quad 0{\cdot}00001 \sin\phi + 0{\cdot}00052 \sin 2\phi$$
$$- 0{\cdot}00016 \cos\phi + 0{\cdot}00073 \cos 2\phi \; . \quad .. \quad .. \quad .. \quad .. \quad .. \quad (7)$$

This variation of rolling moment with bank is similar to those found by Evans and Fink for a number of tunnels to the extent that the harmonic term in 2ϕ is large, but the variation is considerably less than that found by them in the Council of Scientific and Industrial Research 9-ft $\times$ 7-ft tunnel.

To gain some idea of the largest correction applicable to the present series of measurements the following experimental case is considered, since it is the one corresponding to the lowest value of C_l.

For $\xi_0 = 4$ deg and $V = 190$ ft/sec we have $C_l \simeq -0{\cdot}0045$ (from rolling moments measurements referred to in section 13). It is assumed that the correction ε on the periodic time may be adequately expressed by

$$\varepsilon = \sum_1 \frac{A_n^2 + B_n^2}{2C_l^2(1 + 64n^2C_l^2A^2/\rho^2S^2b^6l_p^4)} .$$

Then let

$$\varepsilon' = \sum_1^2 \frac{A_n^2 + B_n^2}{2C_l^2} \; . \quad .. \quad .. \quad .. \quad .. \quad .. \quad .. \quad .. \quad (8)$$

Substitution in equation (8) of the following values as given by equation (7)

$$A_1 = \quad 0{\cdot}00001 \quad A_2 = 0{\cdot}00052$$
$$B_1 = -0{\cdot}00016 \quad B_2 = 0{\cdot}00073$$

and the above value of C_l leads to

$$\varepsilon' = 0{\cdot}02.$$

This means that even for the extreme case of a system of zero inertia the actual periodic time T would be approximately 2 per cent greater than T_0 due to the variation in rolling moment. In the practical case owing to the inertia about the rolling axis the correction is likely to be very much smaller. In view of this no attempt was made to apply corrections to the experimental results.

11. *Modified Model with a Lower Torsional Stiffness.*—An attempt was made to lower the reversal speed to within the speed range of the tunnel by decreasing the torsional stiffnesses of the wings. The modification which was carried out by Messrs. Boulton Paul consisted principally in removing the skins between the main and rear spars and replacing them with sheets that were not cemented to either of the spars but only to the ribs. The modified arrangement is illustrated by Fig. 14, which shows the edge of a skin positioned by, but free to slide between

the spar boom and a butt strap on the outer surface of the wing. This arrangement eliminated the 'torsion box' property of the rear portion of the wing, and the torsional stiffness was correspondingly reduced. In addition some reduction in stiffness was achieved by cutting lightening holes in the web of the main spar.

Torsional stiffnesses were measured, as before, by using a loading template near the wing tip (*i.e.*, at $\eta = 0{\cdot}87$) and measuring the twist by a mirror placed at the main spar at $\eta = 0{\cdot}83$. The new stiffness values were

Port	33 lb ft/radn
Starboard	32 ,, ,,
Mean	32·5 ,,

It will be noticed that even after the modification the wing stiffness was well above the value 24 lb ft/radn calculated from a consideration of the model scales (*see* section 5).

A large disagreement between calculated and measured rolling speeds* for the modified model led to an investigation of the distortion that took place during rolling.

Firstly it was found that the air loads due to aileron deflection caused a wing distortion which involved a change of aerodynamic section. Evidence of this was given by the readings of deflection obtained with a number of small concave mirrors attached to the wing surface at intervals along one chord whilst roll was prevented. The type of distortion that occurred was reproduced under static conditions by applying equal but opposite loads at the main and rear spars respectively, and Fig. 16 shows in an exaggerated form the principal features of this mode of distortion†. The ribs between the main and rear spars might have been expected to prevent a distortion of this nature, but their flanges allowed them to have a slight flexibility in their own planes. As indicated in Fig. 15 this was due partly to the inevitable gradual curvature instead of a right-angle at the flanges, which allowed some amount of 'rolling' to take place, and partly to the tearing action at the cemented joint between the rib flange and the spar web. During the stiffness tests the possibility of this type of distortion occurring was masked by the presence of the contour board at the loading station which prevented any change of section at least at one spanwise position.

An attempt was made, but without success, to eliminate this type of distortion by a few tensioned Xylonite straps joining the main spar to the rear spar. It did not appear possible without a very drastic modification to the wing structure to eliminate the change in section and at the same time retain the reduced torsional stiffness. Although a full-scale aircraft would not distort in this manner, at least not to any appreciable degree, it is considered useful to include an account of the work done with the modified model.

12. *Wind-tunnel tests with the Modified Model.*—Rolling speeds over a range of air speeds were measured as before and the results are shown in Fig. 17. The air speed was not raised above 140 ft/sec since there seemed to be some likelihood that the loads would damage the model. An extrapolation from the graph of $p/\xi_0 V^3$ against $1/V^2$ (Fig. 18) gives the reversal speed as 169 ft/sec. Fig. 17 also includes curves calculated as described in section 23.

Reference has already been made to the characteristic feature of the distortion due to aileron loads, and Fig. 16 includes definitions of the two angles of deflection ψ' and ψ''. Values of these angles were measured whilst the model was rolling by small concave mirrors attached to the undersurface of the wing, at the main spar position for the measurement of ψ', and at the rear spar for ψ''. A point source of light was placed at a window of the tunnel and as the model

* For instance it would be expected from the measured stiffness that the reversal speed would be 216 ft/sec, whilst experimental results suggested that it would be 169 ft/sec.

† Such a distortion is unlikely to have taken place with the unmodified wing due to the constraint of the cemented skin.

rotated each reflected beam of light swept out an arc. For part of each revolution the image at a screen at the tunnel window appeared as a vertical line, the horizontal shift of which was a measure of the wing distortion. To avoid confusion at the screen, measurements were made in pairs, one acting as a reference.

Fig. 19 shows the values of ψ'/ξ_0 and ψ''/ξ_0 measured at two spanwise stations $\eta = 0{\cdot}57$ and $\eta = 0{\cdot}79$ on the port wing. The diagram shows that for each station and particularly for $\eta = 0{\cdot}57$ the rotation ψ'' was considerably greater than ψ'. The diagram also shows linearity of each deflection with V^2, and thus the invariability of the mode with air speed.

Some idea of the spanwise variation of ψ' and ψ'' was obtained by measurements made on both wings for the two aileron conditions $\xi_0 = +10$ deg and -10 deg, and at the nominal speeds $V = 60$, 100, and 140 ft/sec. These measurements confirmed the previous set, in that there was no significant change in the mode of distortion for these air speeds. Fig. 20, which has been prepared by taking the mean of the results at the different air speeds and aileron settings, shows spanwise distortion functions ψ'/ψ''_0 and ψ''/ψ''_0 where ψ''_0 is the value of ψ at the reference section at $\eta = 0{\cdot}57$.

13. *Rolling Moment Measurements.*—Rolling moments due to aileron deflections were measured with the modified model. To avoid any possible interference effects due to the horizontal and vertical struts, these measurements were made with the model set at an angle of bank $\phi = 225$ deg. A preliminary test at 80 ft/sec established the fact that the slope $dC_l/d\xi_0$ was the same for any of the positions $\phi = 45$ deg, 135 deg, 225 deg and 315 deg. Measurements were made at a number of speeds up to 140 ft/sec for a range of aileron angles -10 deg $< \xi_0 < +10$ deg. The rolling-moment coefficient C_l plotted linearly with ξ_0, and values of $dC_l/d\xi_0$ for different air speeds were obtained from the graphs.

Theoretically it would be expected that

$$dC_l/d\xi_0 = (dC_l/d\xi_0)_0 - (\theta_0/\xi_0)k_\theta \quad .. \quad .. \quad .. \quad .. \quad .. \quad .. \quad .. \quad (9)$$

where $(dC_l/d\xi_0)_0$ refers to a similar but rigid system, k_θ involves the mode of distortion of the wings, and θ_0 represents the distortion at some reference station.

With the assumption that the mode of distortion is independent of air speed, and that (θ_0/ξ_0) is proportional to V^2, equation (9) reduces to

$$dC_l/d\xi_0 = (dC_l/d\xi_0)_0 - KV^2 \quad .. \quad .. \quad .. \quad .. \quad .. \quad .. \quad .. \quad (10)$$

where K is a constant.

In Fig. 21 the measured $dC_l/d\xi_0$ is plotted against V^2 and the graph shows reasonable linearity. The results are extrapolated to give a reversal speed of 167 ft/sec which is in good agreement with the value 169 ft/sec obtained by extrapolation from the rolling speed results.

14. *The Value of l_p.*—The following equation represents the condition of steady rolling

$$\tfrac{1}{2}\rho V^2 Sb(dC_l/d\xi_0)\xi_0 = -\tfrac{1}{4}\rho SVb^2 l_p p \quad .. \quad .. \quad .. \quad .. \quad .. \quad (11)$$

so that the coefficient l_p is given by

$$l_p = -(dC_l/d\xi_0)/(ps/\xi_0 V)\,. \quad .. \quad .. \quad .. \quad .. \quad .. \quad .. \quad (12)$$

In Figs. 21 and 22 respectively $dC_l/d\xi_0$ and $ps/\xi_0 V$ are plotted against V^2. The ' least-squares ' straight lines through the points give intercepts at $V^2 = 0$ from which

$$(dC_l/d\xi_0)_0 = -0{\cdot}114$$

$$(ps/\xi_0 V)_0 = -0{\cdot}305.$$

Substitution of these values in equation (12) leads to the result

$$l_p = -0{\cdot}37.$$

In the next section it is suggested that the correction to this value due to tunnel-wall interference is negligible.

The above value of l_p refers to zero or nearly zero resultant lift on the model and compares favourably with the experimental results of Evans and Fink[6] for a model of the *Boomerang* wings extrapolated to the condition $C_L = 0$.

15. *Tunnel-wall Interference.*—No detailed examination of the effect of tunnel-wall interference on the experimental results has been made, but the following consideration suggests that the corrections are not serious.

The resultant spanwise lift distribution for any of the test conditions may be assumed to be antisymmetrical, and in the general case may be regarded as consisting of components due to

(i) ailerons

(ii) wing distortion

(iii) rolling.

The general resultant rolling moment acting in the tunnel may similarly be resolved and written as

$$L = \xi_0 L_\xi + \theta_0 L_\theta + pL_p \quad .. \quad .. \quad .. \quad .. \quad .. \quad .. \quad .. \quad (13)$$

or

$$L = \xi_0 L_\xi'(1 + \varepsilon_\xi) + \theta_0 L_\theta'(1 + \varepsilon_\theta) + pL_p'(1 + \varepsilon_p) \quad .. \quad .. \quad .. \quad (14)$$

where the accented symbols refer to free-air conditions and ε_ξ, ε_θ and ε_p represent the separate corrections due to wall interference. Each of these corrections depends on the distribution but not on the magnitude of the lift component to which it refers. A theoretical investigation of the effect of tunnel wall interference on antisymmetrical lift distributions has been made by Evans[8], and from his results it is concluded that although there are differences between the shapes of the three components lift distributions it is permissible to write

$$\varepsilon_\xi = \varepsilon_\theta = \varepsilon_p = \varepsilon \, .$$

Under the condition of steady rolling in the tunnel the resultant rolling moment L is zero, thus equation (13) becomes

$$0 = \xi_0 L_\xi + \theta_0 L_\theta + pL_p \, ,$$

and equation (14) after division by $(1 + \varepsilon)$ becomes

$$0 = \xi_0 L_\xi' + \theta_0 L_\theta' + pL_p' \, . \quad .. \quad .. \quad .. \quad .. \quad .. \quad .. \quad (15)$$

Equation (15) is identical with that which expresses the steady rolling in free air, and thus there is no wall-interference correction to be applied to the rolling speed as measured in the tunnel.

The results of Evans suggest that ε will not be more than $0 \cdot 02$ for the conditions of the experiments. Thus it is probable that the measured values of $(dC_l/d\xi_0)$ and l_p (since this is obtained from $(dC_l/d\xi_0)$) are numerically not more than 2 per cent in excess of their free-air values.

16. *Calculation of the Rolling Power and Aileron Reversal Speed for the Model.*—Calculations of the rolling power were made by the Collar and Broadbent (CB) iterative method[4], and by a method due to Garner (*see* Appendix) based on lifting-line theory. Calculations of the aileron reversal speed were also made by the semi-rigid method[3], and by the Hirst Approximate method[9]. The results are dealt with in sections which follow.

In the calculations, the following data were taken as applicable to the model.

Torsional stiffness m_θ (measured at $\eta = 0 \cdot 83$) = 63 lb ft/radn.

Mode of torsional distortion $F_s(\eta)$ due to couple applied near the tips as shown in Fig. 9.

Position of flexural axis in chords aft of quarter-chord $e = -0 \cdot 03$.

17. *The Collar and Broadbent (CB) Method.*—The wing was assumed to be divided into 12 strips, five of them being over the extent of the aileron as shown in Fig. 23a. The local torsional stiffnesses per unit length were obtained from the measured torsional displacements due to a couple applied near the tip. In all, five sets of calculations were made involving variations in the aerodynamic

coefficients and the position of the flexural axis as shown in the following table which also gives the calculated reversal speeds.

Calculation	a_2/a_1 and m	a_1	e	V_r
1	0·80(T)	2π	+0·05	306 ft/sec
2	0·80(T)	2π	−0·03	300
3	0·80(T)	2π	−0·15	292
4	0·65(T)	2π	−0·03	300
5	0·80(T)	5·0	−0·03	300

In the above specification of the quantities a_2/a_1 and m, (T) represents the Glauert two-dimensional values ; these were obtained appropriate to the aileron/wing chord ratio, E, of each strip from the curves given by Victory[3].

The results of calculations 1, 2 and 3 are shown in Fig. 24 in the form of rolling power $(ps/\xi_0 V)$ plotted against air speed V ; they show that rolling power is not very sensitive to the position of the flexural axis. Calculation 5 in which a_1 was taken as 5·0 gives a reversal speed equal to that obtained by assuming a_1 is 2π (calculation 2). Thus for the case $e = -0{\cdot}03$ at least, the calculated rolling power is insensitive to the value of a_1 used in the calculation*.

The iterative process involved in the calculation leads to the successive improvement of the estimated mode of twist. The process was initiated with a linear mode, and two iterations led to a satisfactory convergence. The final mode which is shown in Fig. 25 was found to be little changed by air speed, and sensibly the same for all five sets of calculations.

The important aerodynamic quantities are the ratio a_2/a_1 and m, the former being operative in determining the ' rigid-wing ' rolling power $(ps/\xi_0 V)_0$ (*i.e.*, the rolling power of a geometrically similar but rigid wing), whilst the calculated reversal speed may be regarded as dependent on the combination $\sqrt{(a_2/a_1\, m)}$.

If X is the ratio of the rolling power of the actual elastic wing to that of a similar but rigid wing, then

$$X = (ps/\xi_0 V)/(ps/\xi_0 V)_0 = \phi(V) .$$

Both the measurements and the calculations show that the variation of $(ps/\xi_0 V)$ can be regarded as linear with V^2, so that X may be represented by the relation

$$X = \{1 - (V/V_r)^2\}$$

where V_r is the reversal speed.

Fig. 26 shows that the measured and calculated variations of X with V are in agreement, which fact suggests that good prediction of the loss of rolling power is obtained by the use of values of a_2/a_1 and m which are the same proportion of the theoretical two-dimensional values.

The discrepancy between calculation and experiment lies in the ' rigid-wing ' rolling power $(ps/\xi_0 V)_0$, which is directly proportional to the value of a_2/a_1 that is used. In the original calculation values 0·8(T) were chosen on a somewhat arbitrary basis (*see* Ref. 3), whereas the measured rolling powers indicate that the value should be 0·65(T). An estimate of a_2/a_1 using the Royal Aeronautical Society's Data Sheets[12] was made with account taken of the gap between the aileron and wing, and some allowance made for the partial shielding of the balance area, the aileron being of the Frise type (*see* Fig. 7). This estimate leads to a value for a_2/a_1 lying between 0·68(T) and 0·74(T) depending on the extent of the shielding of the balance area ;

* The calculated reversal speed would be affected by the value of a_1 in cases where the separation between the flexural axis and the quarter-chord position is large.

the corresponding range of $(ps/\xi_0 V)_0$ is $-0{\cdot}33$ to $-0{\cdot}36$. The measured values were $-0{\cdot}31$ and $-0{\cdot}305$.

18. *Calculation Based on Lifting-line Theory.*—H. C. Garner has calculated the rolling power for the model wing by an iterative method in which lifting-line theory provides the aerodynamic loadings. An outline of his procedure is given in the Appendix, and the results are shown together with those of CB calculations 2 and 4 in Fig. 27.

The calculated reversal speed is 351 ft/sec, which is considerably greater than that given by other methods, and, although the lifting-line method is more exact than the other methods used, the result is not in good agreement with experiment. However, since the comparison is in effect one between calculation and experiment for one single set of conditions, the lifting-line method should not on account of the disagreement be condemned. The calculated mode of distortion for the reversal condition is shown in Fig. 25.

A calculation in which $(a_2/a_1)_0$ is taken as $0{\cdot}67$(T) yields a value of $(ps/\xi_0 V)_0$ which is in agreement with the measurements. This value may be compared with $0{\cdot}65$(T) required by the strip theory calculation. Thus based on the same value of a_2/a_1 lifting-line theory and strip theory (uncorrected for aspect ratio) give values of $(ps/\xi_0 V)_0$ differing by as little as 3 per cent. This agreement indicates that the aspect ratio correction applicable in the strip theory calculation is small as suggested by the following argument.

The ' rigid-wing ' rate of roll is proportional to the ratio of the rolling moment due to ailerons to the moment due to rolling. That is

$$(ps/\xi_0 V)_0 \propto (dC_l/d\xi_0)/l_p \ .$$

In the calculation of $(ps/\xi_0 V)_0$ by strip theory a correction factor for finite aspect ratio is applicable to both $(dC_l/d\xi_0)$ and l_p. Since $(ps/\xi_0 V)$ is proportional to the ratio of these two quantities, the aspect ratio corrections tend to cancel out, and it is thus possible that the correction applicable to $(ps/\xi_0 V)_0$ may be small.

19. *Reversal Speed by the Semi-rigid Method.*—This method was used in the form described by Victory[3]. The value of the torsional stiffness appropriate to the mid-aileron position was obtained from the twist at this section due to a couple applied near the tip. The method involves an assumption regarding the mode of twist at the reversal condition. Two cases were considered (1) a linear mode, and (2) the mode obtained from the CB calculation given in Fig. 25.

The results of these two calculations are as follows :

	Mode	Reversal speed
(1)	Linear	270 ft/sec
(2)	CB calculation	286 ft/sec

20. *Hirst ' Equivalent Wing ' Method.*—A rapid method of obtaining an approximate estimate of the reversal speed is described by Hirst[9] and Victory[3] in which an equivalent linearly tapered wing of the same span and area is derived. From the geometry of this equivalent wing and the torsional stiffness as measured at the mid-aileron position of the actual wing, the reversal speed may be obtained using the tables and graphs of Ref. 3. It must be pointed out that this method was not intended to apply to a wing of the *Spitfire* type in which (*a*) there is considerable variation in aileron chord ratio along the span or (*b*) the distance between the outer end of the aileron and the wing tip is considerable. Nevertheless as a matter of interest, estimations were carried out

for the complete wing (*see* Fig. 23b) and for a wing in which the tip portion (*i.e.*, the portion of the wing outboard of the aileron) was neglected (*see* Fig. 23c). These results are as follows :

	Reversal speed
Complete wing	258 ft/sec
Wing tip neglected	282 ft/sec

21. *Comparison with Full-scale Results.*—Reversal speeds for the full-scale *Spitfire* V which were obtained by calculation and also by extrapolation from rolling tests are quoted by Victory in Ref. 3. These values have been converted to apply to the model by using the following relation :

$$V_M/V_F = \{(L_F/L_M)^3 \,.\, (m_0)_M/(m_0)_F\}^{1/2}$$

where

$$(m_0)_M/(m_0)_F = 3{\cdot}1 \times 10^{-4}$$

$$L_F/L_M = 7.$$

The following table allows the full-scale and model reversal speeds to be compared.

	Spitfire V full-scale	*Spitfire* V converted to model-scale	Model
By calculation	600 m.p.h. E.A.S.	286 ft/sec	300 ft/sec (CB method)
Deduced from rolling tests	580	277	309

22. *Summary of Results.*—

Derivation	Reversal speed V_r (ft/sec)	' Rigid-wing ' rolling power $(ps/\xi_0 V)_0$
Model tests		
Original model	309	−0·31
Modified model ($e = -0{\cdot}03$)	—	−0·305
Collar and Broadbent method		
a_2/a_1, m 0·8(T)	300	−0·39
0·65(T)	300	−0·31
($e = -0{\cdot}03$)		
Garner method		
$(a_2/a_1)_0$ 0·8 (T)	351	−0·37
0·67(T)	351	−0·31
($e = -0{\cdot}03$)		
Semi-rigid method		
Linear mode	270	—
(CB) mode	286	—
Hirst ' Equivalent Wing ' method		
Complete wing	258	—
Wing tip neglected	282	—
Conversion from full-scale		
Calculation	286	—
Rolling tests	277	—

23. *Calculated Results for the Modified Model*—In the following calculation made to correlate the measured rolling speeds with the measured wing distortions occurring with the modified model a very simple allowance is made for the change of aerodynamic section. The lift due to wing distortion is assumed proportional to ψ'', the angle of deflection of the rear portion of the wing (*see* Fig. 16). In other words, the wing twist θ of usual theory is replaced by ψ'', whilst the rotation ψ' of the nose portion is ignored.

For the case of steady rolling, following usual theory, the increment in the lift coefficient appropriate to a strip $d\eta$ of one wing is given by

$$C_L = a_1(\psi'' + ps\eta/V) + a_2\xi \quad . \quad . \quad . \quad . \quad . \quad . \quad . \quad . \quad (16)$$

Since for steady rolling the total rolling moment on each wing vanishes

$$0 = L = \tfrac{1}{2}\rho V^2 s^2 \int_0^{1\cdot0} C_L c\eta \, d\eta \quad . \quad . \quad . \quad . \quad . \quad . \quad . \quad . \quad (17)$$

If the aileron is regarded as rigid the local aileron angle is given by

$$\xi = \xi_0 + \psi''_0 - \psi''. \quad . \quad . \quad . \quad . \quad . \quad . \quad . \quad . \quad (18)$$

Let $\psi'' = \psi''_0 f(\eta)$,

then from equations (16), (17) and (18),

$$0 = \int_0^{1\cdot0} [a_1\{\psi''_0 f(\eta) + ps\eta/V\} + a_2\{\xi_0 + \psi''_0(1 - f(\eta))\}]c\eta \, d\eta \quad . \quad . \quad (19)$$

from which, if a_1 is treated as a constant over the span,

$$-\frac{ps}{\xi_0 V} = \frac{\int_0^{1\cdot0} (a_2/a_1)\, c\eta \, d\eta + (\psi''_0/\xi_0)\int_0^{1\cdot0} \{f(\eta) + (a_2/a_1)(1 - f(\eta))\}\, c\eta \, d\eta}{\int_0^{1\cdot0} c\eta^2 \, d\eta} \quad . \quad . \quad . \quad (20)$$

This equation may be used to calculate the rolling power from the known distortion.

Fig. 19 gives the value of ψ''_0/ξ_0 as $-7{\cdot}45 \times 10^{-6}V^2$, and the modal function $f(\eta)$ is given by Fig. 20.

The integrations on the right-hand side of equation (20) were performed by tabular summation over 12 spanwise strips (5 over the aileron) and two sets of values for a_2/a_1 were used.

(*a*) a_2/a_1 taken as 0·80T, calculation yields

$$ps/\xi_0 V = 0{\cdot}387 - 0{\cdot}108 \times 10^{-4}V^2 \quad . \quad . \quad . \quad . \quad . \quad . \quad (21)$$

which gives

$V_r = 190$ ft/sec.

(*b*) a_2/a_1 taken as 0·65T, calculation yields

$$ps/\xi_0 V = 0{\cdot}314 - 0{\cdot}108 \times 10^{-4}V^2 \quad . \quad . \quad . \quad . \quad . \quad . \quad (22)$$

which gives

$V_r = 170$ ft/sec.

The above results are shown plotted in Fig. 17. Calculation (*b*) shows good agreement with experiment and thus confirms the conclusion of section 17, that the values of a_2/a_1 and m appropriate to the model are 0·65(T).

It will be noticed that the coefficients of V^2 in equations (21) and (22) are the same to three significant figures. This is due to there being no appreciable effect from the variation in local angle ξ over the extent of the aileron.

24. *Conclusions.*—(*a*) *Concerning the use of Xylonite models.*—(i) Xylonite is a useful material for the construction of aero-elastic models where some better representation is required than is offered by the type of model consisting of a wooden framework covered with silk.

(ii) The discrepancy between the actual stiffness of the model and that estimated from full-scale suggests that, when a replica of a full-scale structure is required, considerable care will have to be taken to ensure that the stiffness of the model is truly representative of full-scale.

(iii) To achieve a reasonable aerodynamic surface the thickness of the skin of the model should not be below a minimum, which, for the normal size of model is probably in the region 0·010 to 0·015 inches.

(iv) Due to the limitation of (iii) above, Xylonite models are likely to be too stiff for aero-elastic effects to be adequately manifested in the tunnels commonly available. (*i.e.*, 9-ft × 7-ft, 230 ft/sec).

(v) The disadvantages mentioned in (iv) above will tend to disappear as tunnel speed and model size or both are increased, and it is probably in the field of high speeds that Xylonite static aero-elastic and flutter models will have their greatest use.

(*b*) *Concerning the loss of rolling power.*—(i) Experiment and calculation both confirm that loss of rolling power may be expressed by the formula

$$X = 1 - (V/V_r)^2$$

where X is the ratio of the actual rolling power to that of a similar but rigid wing.

(ii) A Collar and Broadbent calculation yields a reversal speed that agrees with the measurements when based on values of (a_2/a_1) and m which are obtained by reducing the theoretical two-dimensional values by the same factor.

(iii) A method of calculation based on lifting-line theory gives a reversal speed in excess of that indicated by the experiments.

(iv) The semi-rigid and the Hirst ' equivalent wing ' methods both give reversal speeds lower than that indicated by the experiments.

(v) The ' rigid wing ' rolling power for the model is correctly estimated by :

(A) *the strip theory* of the Collar and Broadbent calculation when the aerodynamic quantity a_2/a_1 is taken as 0·65 times the two-dimensional theoretical value.

(B) *lifting-line theory* when a_2/a_1 is taken as 0·67 times the two-dimensional theoretical values.

The Royal Aeronautical Society's Data Sheets suggest that a_2/a_1 for the model should lie between 0·68 and 0·74 times the two-dimensional theoretical value. The fact that the value indicated by the experiments lies outside this range may be due to the waviness over the surface of the model wing.

25. *Acknowledgements.*—Acknowledgements are due to Dr. S. C. Redshaw and his staff at Messrs. Boulton Paul for their co-operation throughout the work ; to Mr. E. G. Broadbent of the Royal Aircraft Establishment for advice during the designing of the experiments ; also to Mr. D. B. Betts who assisted in many of the measurements.

REFERENCES

No.	Author	Title, etc.
1	S. C. Redshaw and R. E. Arthur ..	A method of investigating the stiffness of a structure by means of a Xylonite model. Boulton Paul Aircraft Ltd., Tech. Report 15. A.R.C. 7432. December, 1943.
2	S. C. Redshaw	A note on the use of models for aeroplane flutter analysis. Boulton Paul Aircraft Ltd., Tech. Report 16. A.R.C. 7653. 1944.
3	Mary Victory	The calculation of aileron reversal speed. R. & M. 2059. March, 1943.
4	A. R. Collar and E. G. Broadbent ..	The rolling power of an elastic wing. Part I: Compressibility effects absent. R. & M. 2186. May, 1945.
5	Lawton, Carswell and Nason	Effect of some environmental conditions on the mechanical properties of cellulose acetate and cellulose nitrate plastic sheets. *Trans. A.S.M.E.*, Vol. 68, No. 1. January, 1946.
6	J. M. Evans and P. T. Fink	Determination of l_p by free rolling. C.S.I.R. Division of Aeronautics Report A.43. August, 1946. Communicated by Prof. A. V. Stephens, Dept. of Aeronautical Engineering, University of Sydney. A.R.C. 10,765.
7	A. B. Pugsley and H. Roxbee Cox ..	The aileron power of a monoplane. R. & M. 1640. April, 1934.
8	J. M. Evans	Wind-tunnel interference on the lateral derivatives l_p, l_r and l_v with particular reference to l_p. C.S.I.R. Report A.41.
9	D. M. Hirst	On the calculation of the critical reversal speeds of wings. With an Appendix on rolling moment induction factors by G. R. Brooke and D. M. Hirst. R. & M. 1568. September, 1933.
10	H. Multhopp	The calculation of the lift distribution of aerofoils. R.T.P. Translation No. 2392. A.R.C. 8516.
11	L. W. Bryant, A. S. Halliday and A. S. Batson.	Two-dimensional control characteristics. R. & M. 2730. April, 1950.
12	.. ..	Royal Aeronautical Society Data Sheets (Aerodynamics). Fourth Issue. September, 1949.

APPENDIX

By

H. C. GARNER

Application of lifting line theory

Multhopp's[10] form of the lifting-line theory for unswept wings is readily applicable to the aeroelastic problem of aileron reversal.

The model wing (Fig. 6) is assumed for this purpose to have an elliptic distribution of chord, such that

$$s = \text{semi-span} = 2{\cdot}649 \text{ ft}$$

$$c_r = \text{root chord} = 1{\cdot}182 \text{ ft}$$

$$S = \tfrac{1}{2}\pi c_r s = \text{gross wing area} = 4{\cdot}919 \text{ sq ft.}$$

The aileron is of spanwise extent $0{\cdot}4970 < \eta < 0{\cdot}8718$, its angle of deflection ξ_0 being referred to the station $\eta = 0{\cdot}5738$. The two-dimensional lift slope is taken to be a constant $a_1 = 5{\cdot}244$ along the whole span.

The spanwise distribution of lift falls conveniently into four contributions due to :

(*a*) initial constant aileron deflections $\xi = \pm \xi_0$

(*b*) effect of rotation in roll $\alpha = + py/V$

(*c*) wing twist due to elasticity $\theta = F_D(\eta)\theta_0$

where $F_D(\eta) = 1$ at the reference station $\eta = 0{\cdot}5738$, at which the aileron is locked to the wing

(*d*) correction to ξ, since the aileron does not distort, $\Delta\xi = \theta_0(1 - F_D)$.

The loadings (*a*) and (*d*) depend on the spanwise distribution of a_2/a_1. It is assumed that the two-dimensional values of a_2/a_1, for the Frise aileron are proportional to those for a plain aileron of the same chord ratio E. Thus

$$\frac{a_2}{a_1} = \left(\frac{a_2}{a_1}\right)_0 G(\eta) , \qquad \ldots\ldots\ldots\ldots\ldots\ldots\ldots\ldots \quad (1)$$

where $(a_2/a_1)_0$ denotes an unknown value at the reference station and the distribution $G(\eta)$ is determined for a plain aileron from Ref. 11 (Bryant).

By the principle described in Ref. 4 (Collar and Broadbent) the wing twist is related to the aerodynamic loading by

$$\theta_0 F_D(\eta) = \frac{\frac{1}{2}\rho V^2 s^3}{m_\theta} \int_0^\eta \frac{dF_s}{d\eta} \int_\eta^1 \left(\frac{c}{s}\right)^2 C_m \, d\eta \, d\eta$$

where m_0 = torsional stiffness = 63 lb ft/radn,

$F_s(\eta)$ is the static mode of twist given in Fig. 9,

C_m is the pitching-moment coefficient about the flexural axis at 0·22-chord from the leading edge.

Thus in radians

$$\theta_0 F_D(\eta) = 3{\cdot}509 \left(\frac{V}{100}\right)^2 \int_0^\eta \frac{dF_s}{d\eta} \int_\eta^1 \left(\frac{c}{s}\right)^2 C_m \, d\eta \, d\eta , \qquad \ldots\ldots\ldots\ldots \quad (2)$$

where V is the wind speed in ft/sec.

Since F_D is needed to determine the spanwise loading, the values in Fig. 25 obtained from the (CB) calculation, are used as a first approximation.

The non-dimensional parameter

$$\gamma = \frac{\text{Circulation}}{2sV}$$

is calculated by lifting-line theory[10] ($m = 15$) for the following antisymmetrical distributions of incidence using $a_1 = 5{\cdot}244$:

(*a*) $G(\eta)$ over the aileron $0{\cdot}4970 < \eta < 0{\cdot}8718$, 0 elsewhere

(*b*) η along the whole span

(*c*) $F_D(\eta)$ along the whole span

(*d*) $G(\eta)\{1 - F_D(\eta)\}$ over the aileron, 0 elsewhere.

Hence

$$\gamma = \left(\frac{a_2}{a_1}\right)_0 \xi_0 \gamma_a + \frac{ps}{V} \gamma_b + \theta_0 \gamma_c + \theta_0 \left(\frac{a_2}{a_1}\right)_0 \gamma_d , \qquad \ldots\ldots\ldots\ldots \quad (3)$$

where in terms of $\phi = \cos^{-1}\eta$ the values are

First Approximation

ϕ (deg)	F_D	G eq. (1)	$G(1-F_D)$	γ_a	γ_b	γ_c	γ_d
$11\frac{1}{4}$	1·479	0	0	0·0175	0·0706	0·1119	−0·0054
$22\frac{1}{2}$	1·479	0	0	0·0477	0·1305	0·2148	−0·0155
$33\frac{3}{4}$	1·465	0·809	−0·376	0·1512	0·1705	0·2951	−0·0548
45	1·301	1·005	−0·303	0·2223	0·1845	0·3249	−0·0569
$56\frac{1}{4}$	0·951	0·990	+0·049	0·2108	0·1705	0·2838	−0·0144
$67\frac{1}{2}$	0·495	0	0	0·0594	0·1305	0·1854	−0·0077
$78\frac{3}{4}$	0·161	0	0	0·0212	0·0706	0·0817	−0·0027
90	0	0	0	0	0	0	0

It should be noted that the limiting values of $G(\eta)$ are

$$\left.\begin{aligned} G(0{\cdot}4970) &= 0{\cdot}950 \text{ at } \phi = 60{\cdot}2 \text{ deg} \\ G(0{\cdot}8718) &= 0{\cdot}663 \text{ at } \phi = 29{\cdot}3 \text{ deg} \end{aligned}\right\}$$

The values of γ_a, γ_b are now known, but the values of γ_c, γ_d are dependent on F_D which must be evaluated from equation (2).

For convenience the function $F_s(\eta)$ (Fig. 9) is approximately represented by

$$F(\eta) = 0{\cdot}99 \log_{10} \frac{26{\cdot}5}{29 - \eta s} \text{ where } s = 31{\cdot}79 \text{ in.}$$

Then

$$\left.\begin{aligned} \frac{dF}{d\eta} &= \frac{0{\cdot}430}{0{\cdot}9122 - \eta} \quad \text{for } 0{\cdot}0786 < \eta < 0{\cdot}8718 \\ &= 0 \qquad\qquad \text{for } 0 < \eta < 0{\cdot}0786\,;\ 0{\cdot}8718 < \eta < 1 \end{aligned}\right\} \quad \ldots \qquad (4)$$

It remains to determine C_m about the 0·22-chord axis. Since the two-dimensional aerodynamic centre is very close to this axis the contributions to C from γ_b and γ_c (without aileron deflections) are ignored. It is estimated that the local centre of pressure due to the flap contributions γ_a and γ_d occurs at a distance lc from the leading edge where

$$l = 0{\cdot}300 + 0{\cdot}264 \sin^4 2\phi \ . \qquad \ldots \qquad (5)$$

Since $c = c_r \sin\phi$, it follows from equations (3) and (5) that

$$\int_\eta^1 \left(\frac{c}{s}\right)^2 C_m \, d\eta = -\int_\eta^1 \left(\frac{c}{s}\right)^2 \frac{4s\gamma'}{c} (l - 0{\cdot}22)\, d\eta$$

$$= -\frac{4c_r}{s} \int_\eta^1 \gamma' \sin\phi \, (0{\cdot}080 + 0{\cdot}264 \sin^4 2\phi)\, d\eta \ , \qquad \ldots \qquad (6)$$

where

$$\gamma' = \left(\frac{a_2}{a_1}\right)_0 \xi_0 \gamma_a + \theta_0 \left(\frac{a_2}{a_0}\right)_0 \gamma_d \ .$$

Then from equations (2), (4) and (6),

$$\theta_0 F_D(\eta) = -3{\cdot}509\left(\frac{V}{100}\right)^2\left[0{\cdot}99\log_{10}\frac{26{\cdot}5}{29-31{\cdot}79\eta}\int_\eta^1 \frac{4\gamma' c_r}{s}\sin\phi\,(0{\cdot}080+0{\cdot}264\sin^4 2\phi)\,d\eta\right.$$

$$\left.+\int_{0{\cdot}0786}^{\eta} 0{\cdot}99\left\{\log_{10}\frac{26{\cdot}5}{29-31{\cdot}79\eta}\right\}\frac{4\gamma' c_r}{s}\sin\phi\,(0{\cdot}080+0{\cdot}264\sin^4 2\phi)\,d\eta\right]. \quad .. \quad (7)$$

Numerical calculations from equation (7) show that F_D is substantially the same when the term γ_a in the expression for γ' is omitted. The values of F_D so obtained are represented by the dotted curve in Fig. 25. When this second approximation to F_D is used, recalculated values are as follows:

Second Approximation

ϕ (deg)	F_D	$G(1-F_D)$	γ_c	γ_d	$\sin 2\phi$
$11\frac{1}{4}$	1·479	0	0·1121	−0·0054	0·3827
$22\frac{1}{2}$	1·479	0	0·2151	−0·0154	0·7071
$33\frac{3}{4}$	1·465	−0·376	0·2959	−0·0547	0·9239
45	1·301	−0·303	0·3263	−0·0566	1·0000
$56\frac{1}{4}$	0·955	+0·045	0·2877	−0·0138	0·9239
$67\frac{1}{2}$	0·543	0	0·1960	−0·0070	0·7071
$78\frac{3}{4}$	0·185	0	0·0886	−0·0026	0·3827
90	0	0	0	0	0

Since the mode of distortion $F_D(\eta)$ is mainly dependent on γ_a, which is itself independent of F_D, there is no need to proceed to a third approximation to F_D.

Under the conditions of test the model is rolling at a constant rate p and the rolling moment is zero. The coefficient of rolling moment is readily evaluated from equation (3) in the form

$$C_l = \left(\frac{a_2}{a_1}\right)_0 \xi_0 (C_l)_a + \frac{ps}{V}(C_l)_b + \theta_0 (C_l)_c + \theta_0\left(\frac{a_2}{a_1}\right)(C_l)_d \quad .. \quad .. \quad .. \quad (8)$$

where $$(C_l)_a = \frac{2s^2}{S}\left[\frac{\pi}{16}\Sigma\,\gamma_a \sin 2\phi\right]$$

and $(C_l)_b$, $(C_l)_c$, $(C_l)_d$ are given by similar expressions.

Thus

$$\frac{S}{2s^2}(C_l)_a = \quad 0{\cdot}1271$$

$$\frac{S}{2s^2}(C_l)_b = \quad 0{\cdot}1449$$

$$\frac{S}{2s^2}(C_l)_c = \quad 0{\cdot}2421$$

$$\frac{S}{2s^2}(C_l)_d = -0{\cdot}0273.$$

The condition $C_l = 0$ therefore gives

$$0{\cdot}1271\left(\frac{a_2}{a_1}\right)_0 \xi_0 + 0{\cdot}1449\frac{ps}{V} + 0{\cdot}2421\theta_0 - 0{\cdot}0273\theta_0\left(\frac{a_2}{a_1}\right)_0 = 0\,. \quad .. \quad (9)$$

By numerical evaluation of equation (7) at the reference station

$$\theta_0 = -3{\cdot}509\left(\frac{V}{100}\right)^2\left[0{\cdot}0122\left(\frac{a_2}{a_1}\right)_0 \xi_0 - 0{\cdot}0025\left(\frac{a_2}{a_1}\right)_0 \theta_0\right]. \quad .. \quad .. \quad (10)$$

On eliminating θ_0 from equations (9) and (10),

$$-0{\cdot}1449\frac{ps}{\xi_0 V} = 0{\cdot}1271\left(\frac{a_2}{a_1}\right)_0 - 0{\cdot}0427\left(\frac{a_2}{a_1}\right)_0\left(\frac{V}{100}\right)^2 \frac{0{\cdot}2421 - 0{\cdot}0273\left(\frac{a_2}{a_1}\right)_0}{1 - 0{\cdot}0089\left(\frac{a_2}{a_1}\right)_0\left(\frac{V}{100}\right)^2}$$

$$= \left(\frac{a_2}{a_1}\right)_0 \frac{0{\cdot}1271 - 0{\cdot}0103_4\left(\frac{V}{100}\right)^2 + 0{\cdot}0000_4\left(\frac{a_2}{a_1}\right)_0\left(\frac{V}{100}\right)^2}{1 - 0{\cdot}0089\left(\frac{a_2}{a_1}\right)_0\left(\frac{V}{100}\right)^2}\,. \quad .. \quad (11)$$

It follows from equation (11) that the ' initial ' rolling power

$$-\left(\frac{ps}{\xi_0 V}\right)_0 = 0{\cdot}877\left(\frac{a_2}{a_1}\right)_0, \quad .. \quad .. \quad .. \quad .. \quad .. \quad .. \quad .. \quad .. \quad (12)$$

and the reversal speed [virtually independent of $(a_2/a_1)_0$] is

$$V = 100\sqrt{\left\{\frac{0{\cdot}1271}{0{\cdot}0103_4}\right\}} = 351 \text{ ft/sec}\,.$$

The two-dimensional value of a_2/a_1, by Glauert's hinged-plate theory is

$(a_2/a_1)_T = 0{\cdot}525$ at the reference station where $E = 0{\cdot}182$.

If $$\left(\frac{a_2}{a_1}\right)_0 = 0{\cdot}8\left(\frac{a_2}{a_1}\right)_T = 0{\cdot}420\,,$$

the ' initial ' rolling power is calculated to be

$$\left(\frac{ps}{\xi V}\right)_{V=0} = -0{\cdot}368\,.$$

The experimental value of $-0{\cdot}31$ corresponds to the condition

$$\left(\frac{a_2}{a_1}\right)_0 = 0{\cdot}67\left(\frac{a_2}{a_1}\right)_T = 0{\cdot}353\,.$$

As mentioned in section 17 the ratio of the empirical and theoretical values of $(a_2/a_1)_0$ given by the Royal Aeronautical Society Data Sheets (Ref. 12) is between 0·68 and 0·74 depending on the extent of the shielding of the Frise balance. This ratio may be compared with 0·67, for which equation (12) is consistent with the experiments, and with the value 0·8 suggested in Ref. 3.

The curves of $-ps/\xi_0 V$ against V in Fig. 27 include the effect of varying $(a_2/a_1)_0$ and show that the calculated reversal speed of 351 ft/sec is considerably greater than that indicated by experiment and by the method of Collar and Broadbent.

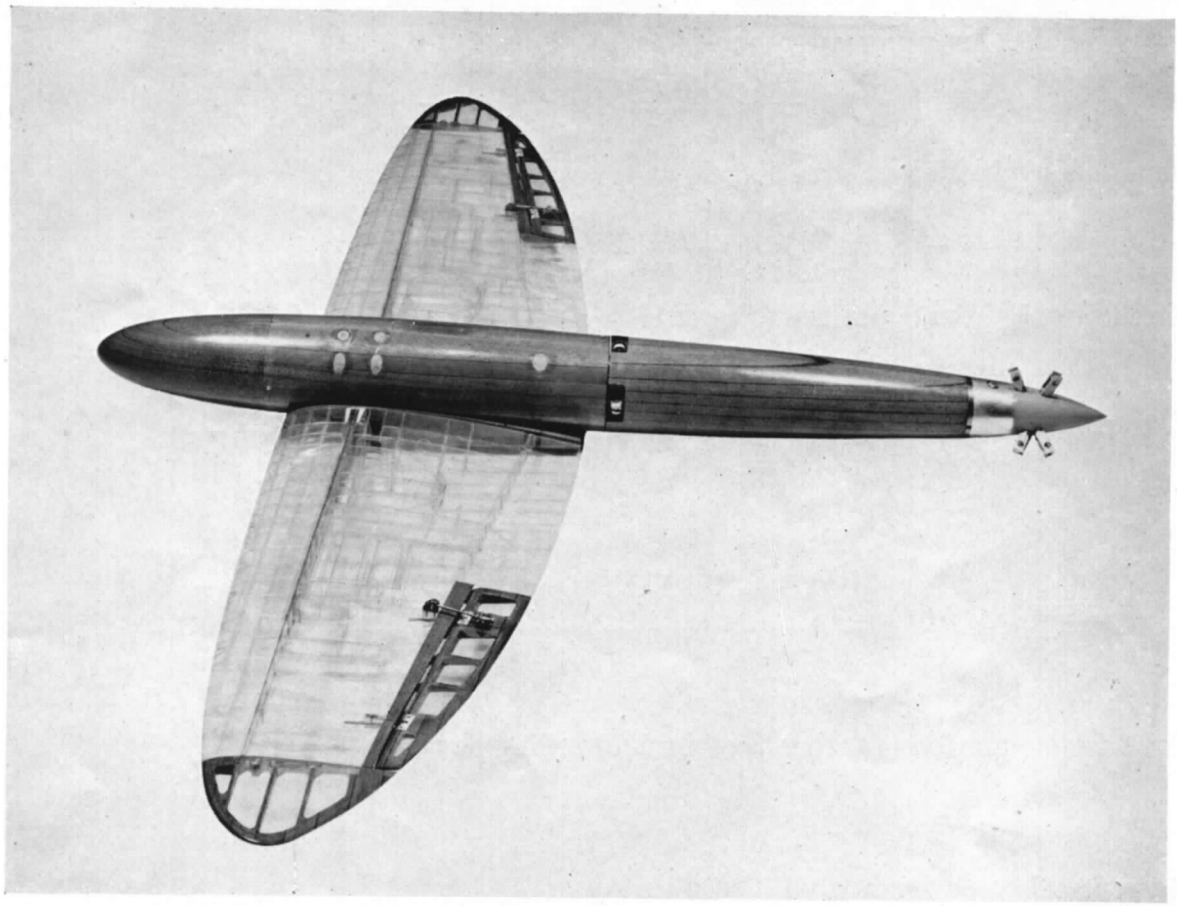

FIG. 1. General view of model.

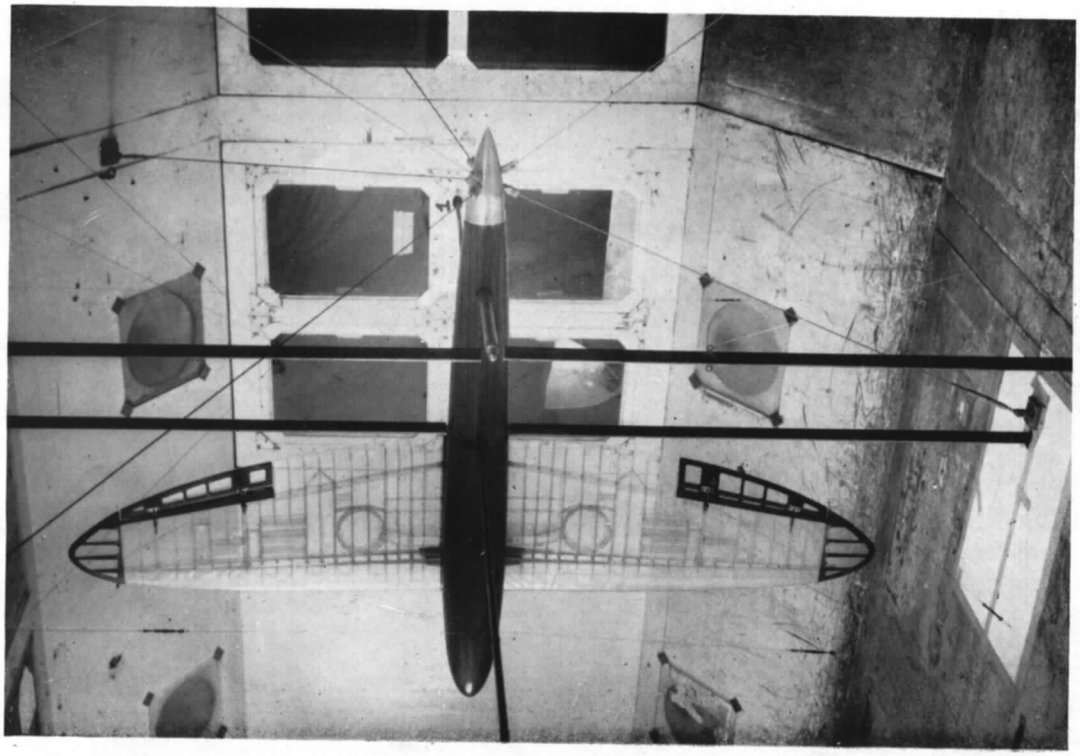

FIG. 2. Arrangement of model in tunnel

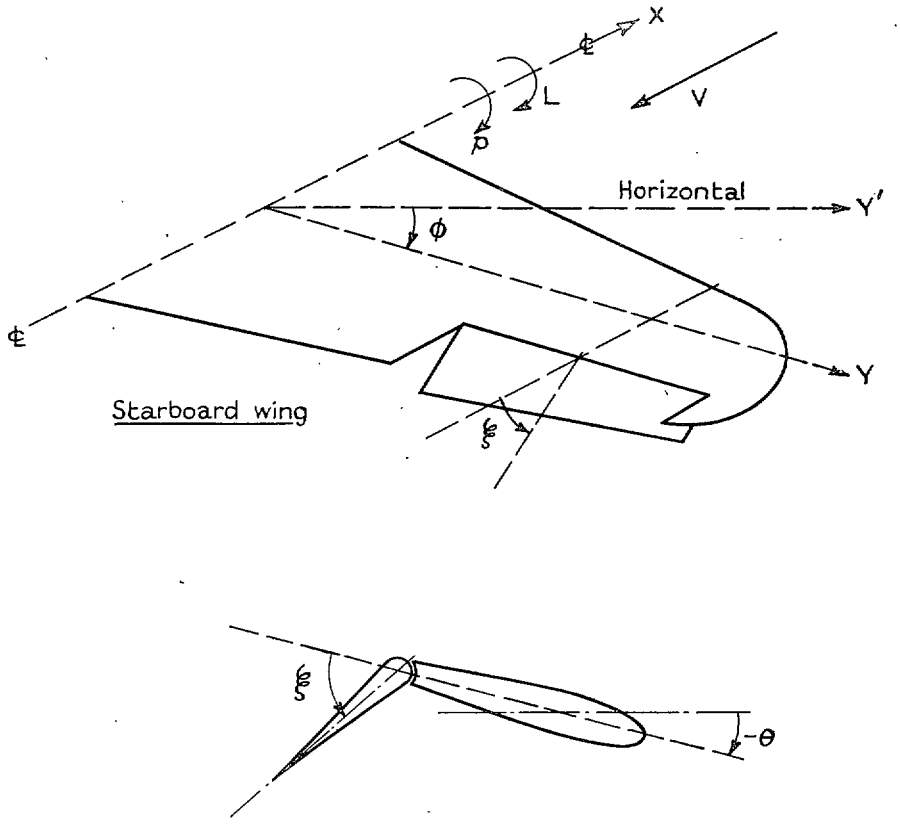

FIG. 3. System of notation.

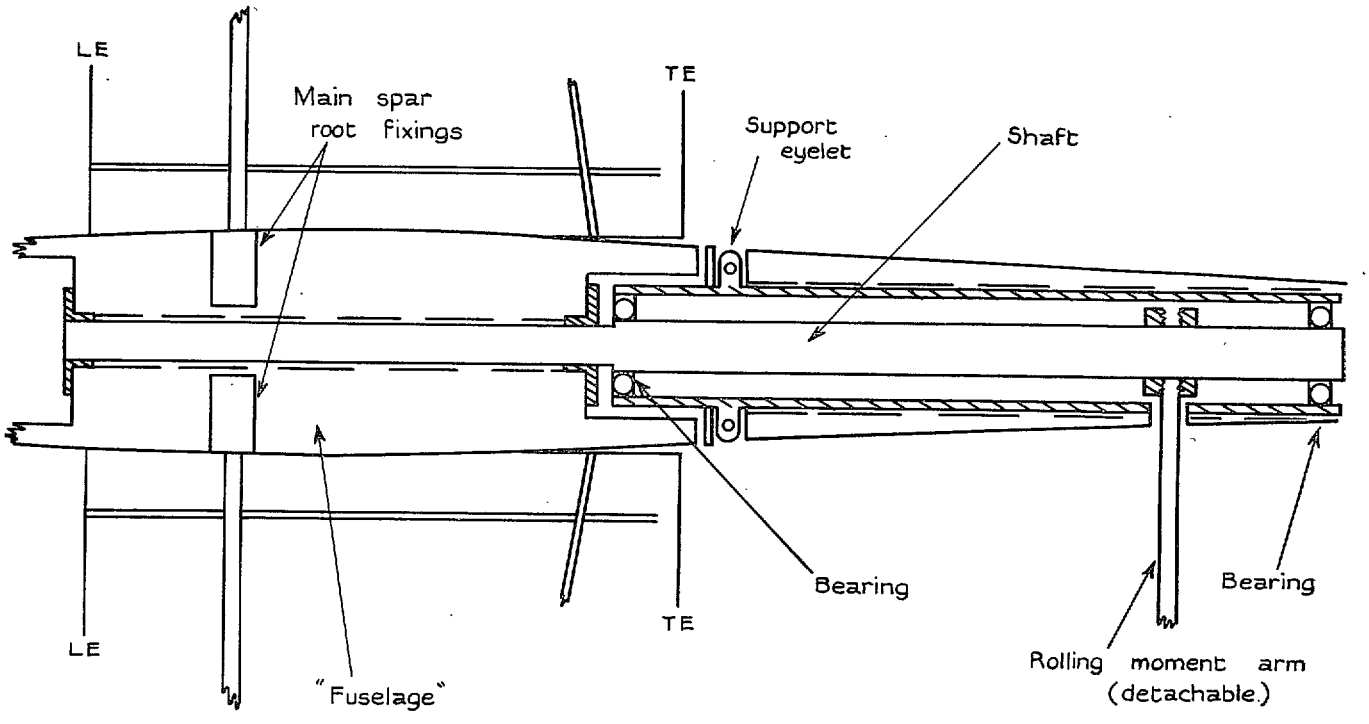

FIG. 4. Arrangement of shaft and bearings forming the rolling axis.

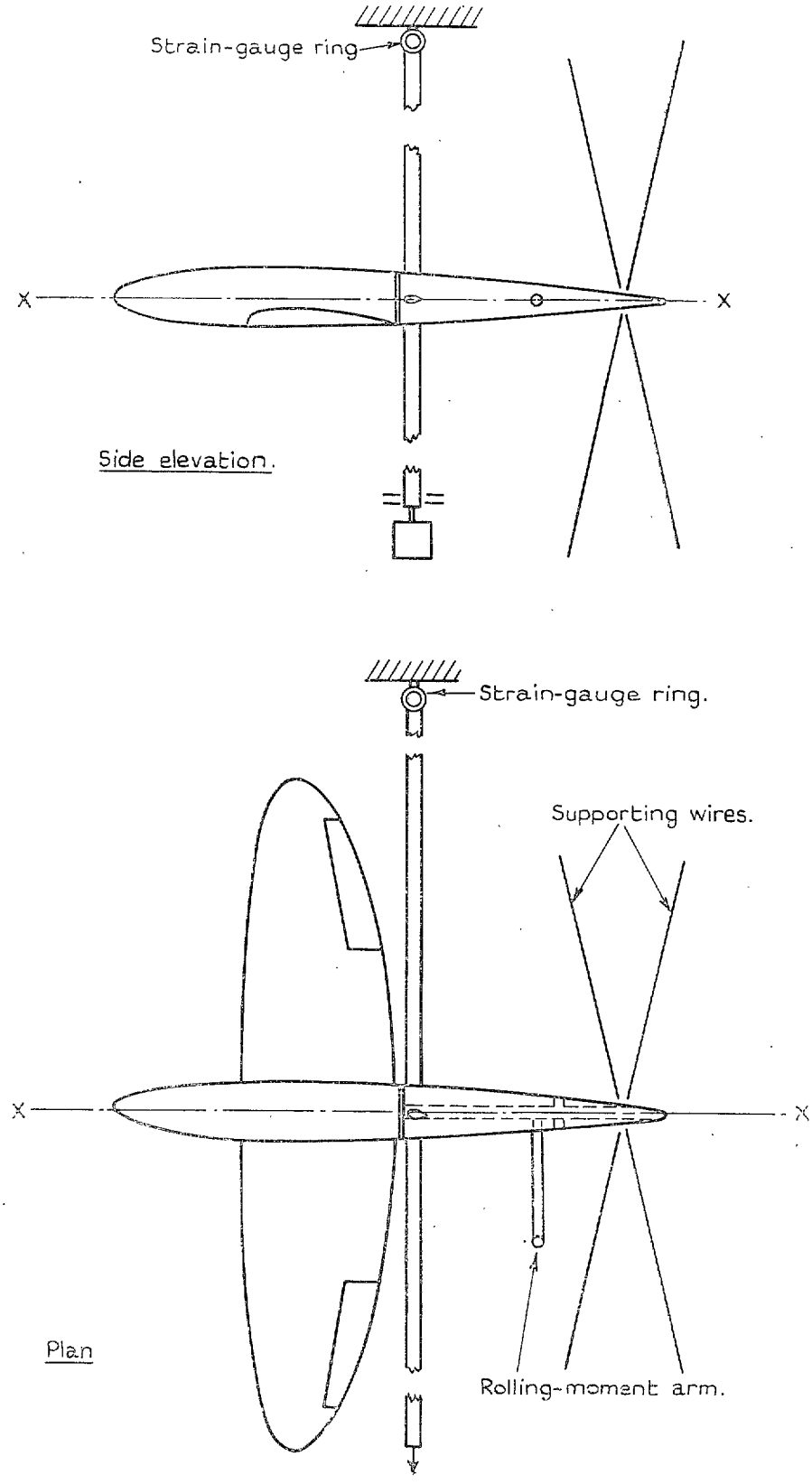

FIG. 5. Arrangement of model in tunnel.

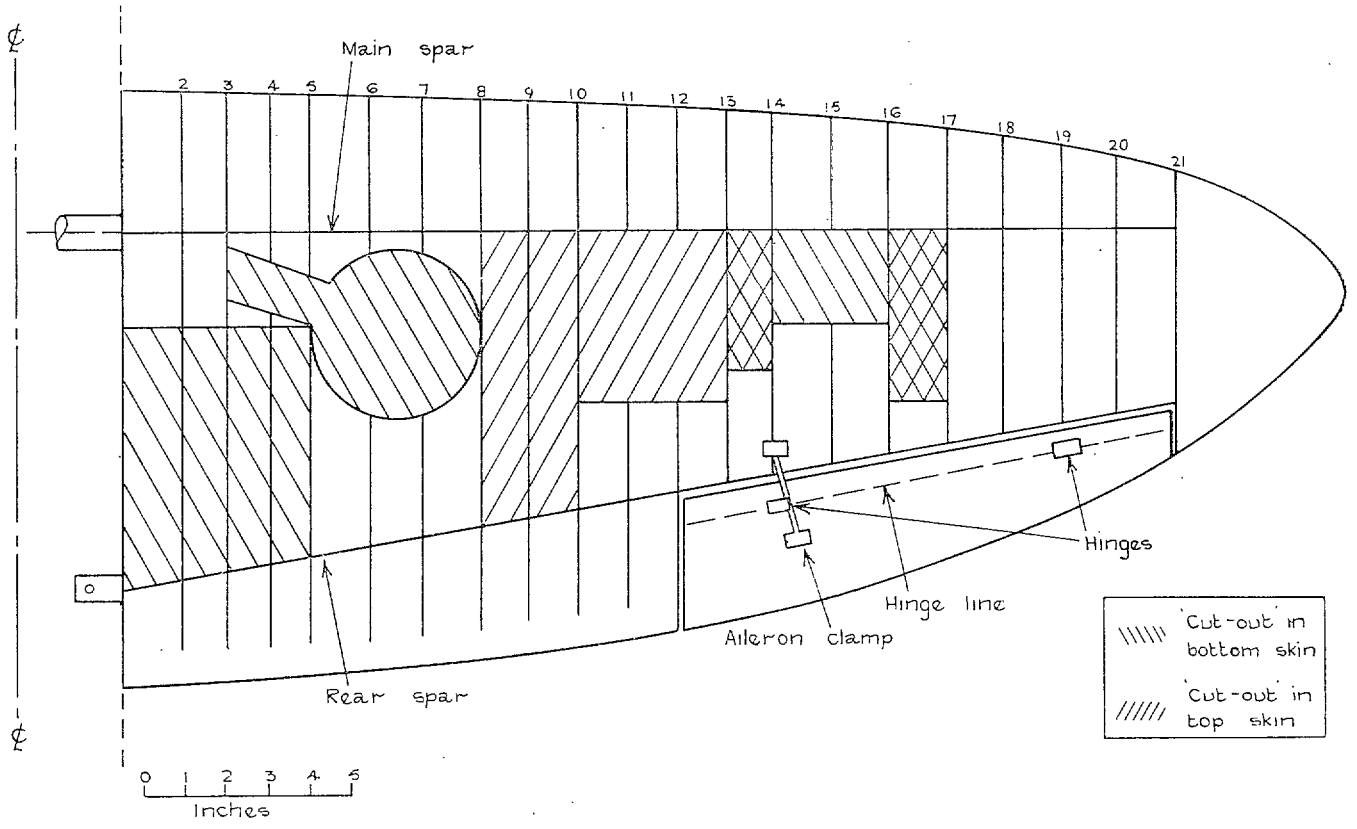

FIG. 6. Diagram of wing showing position of spars, ribs and main ' cut-outs.'

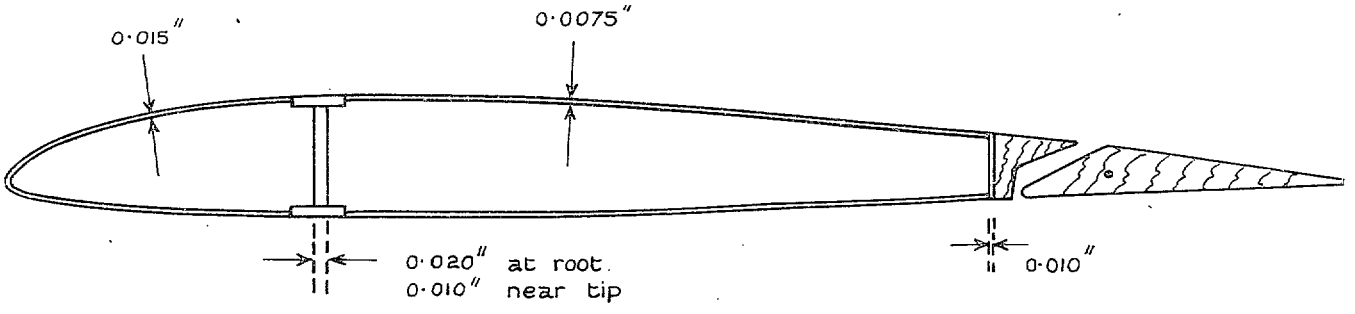

FIG. 7. Main structural features of wings.

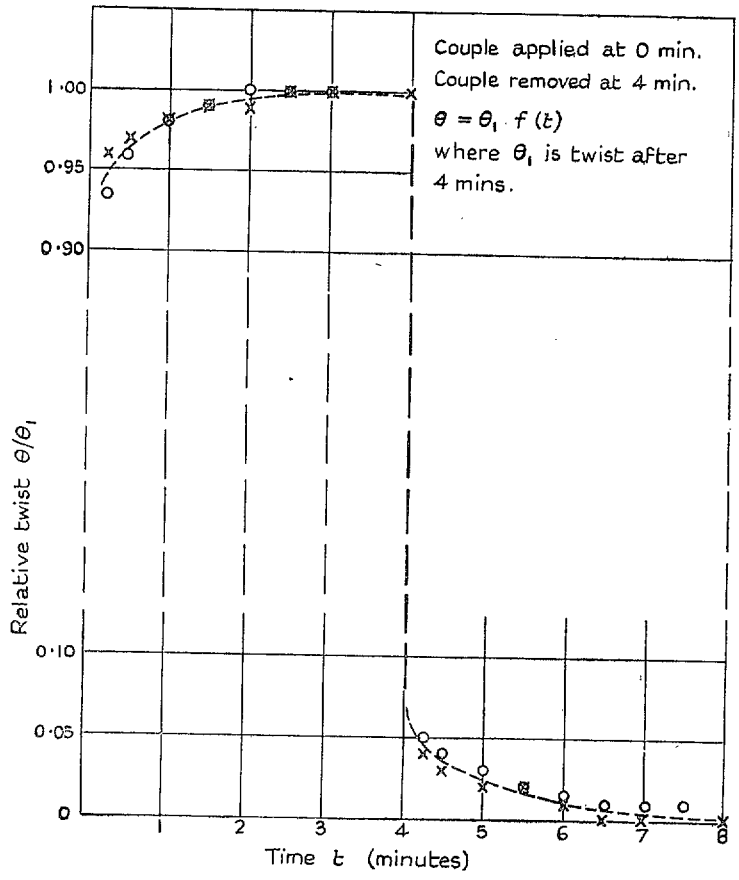

FIG. 8. Creep of torsional distortion for a medium-sized couple applied and then removed.

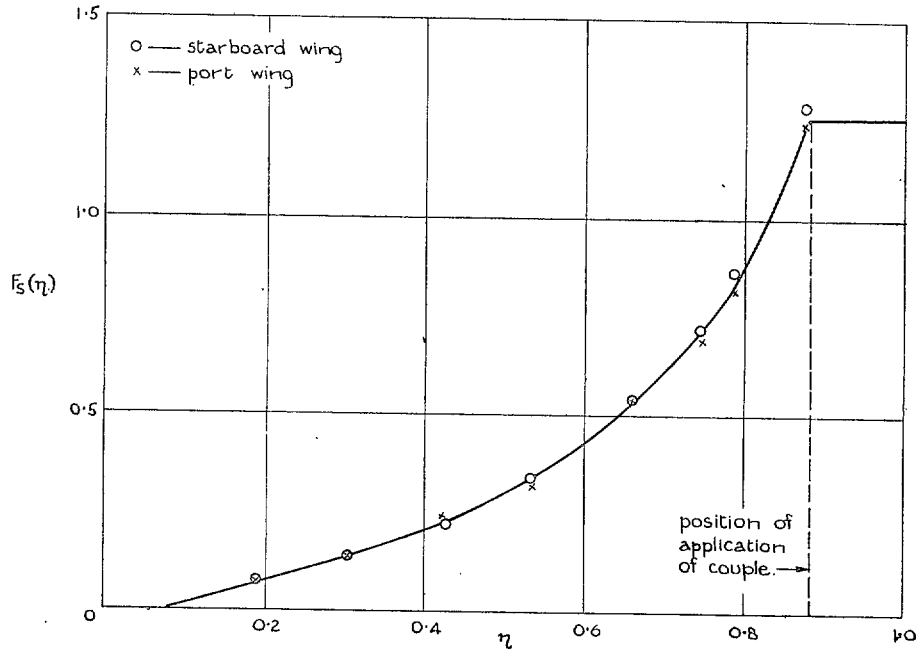

FIG. 9. Measured mode of twist for couple applied at $\eta = 0{\cdot}87$ (rib 21).

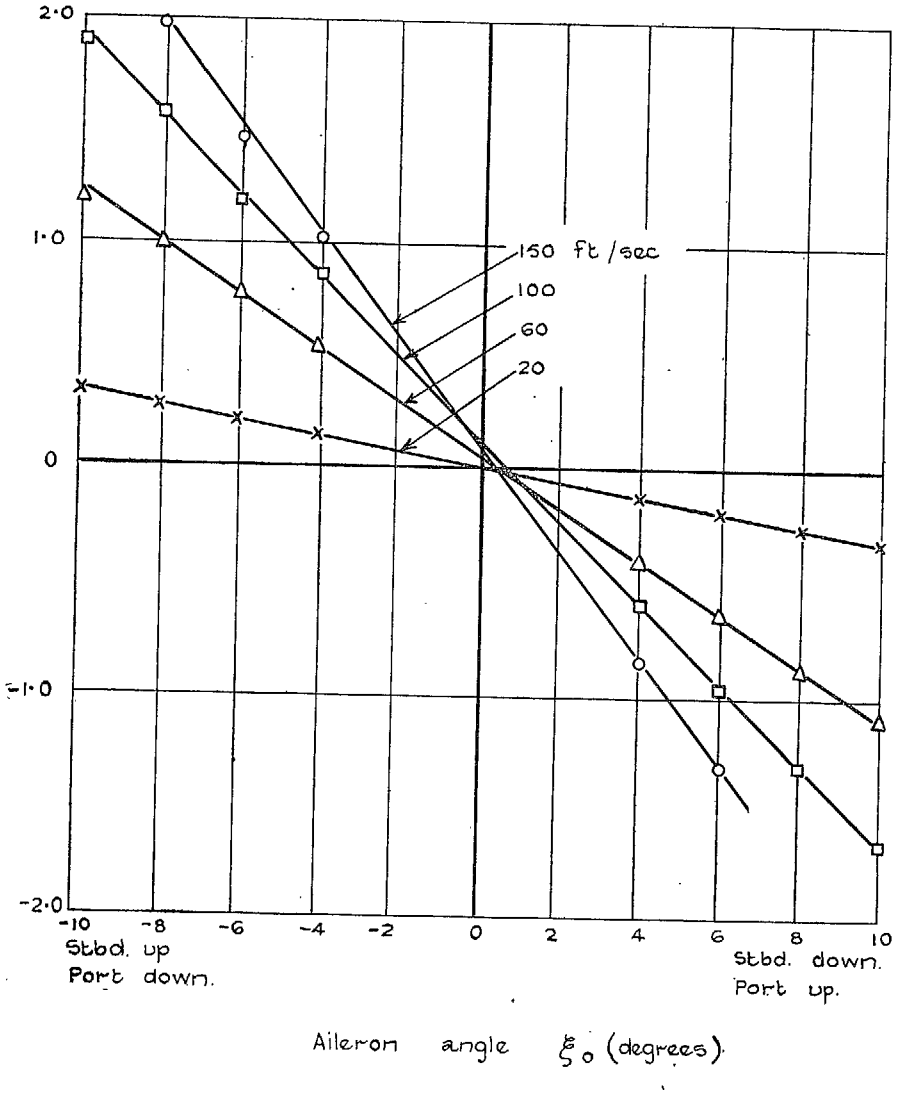

FIG. 10. Variation of rolling speed with aileron angle and air speed.

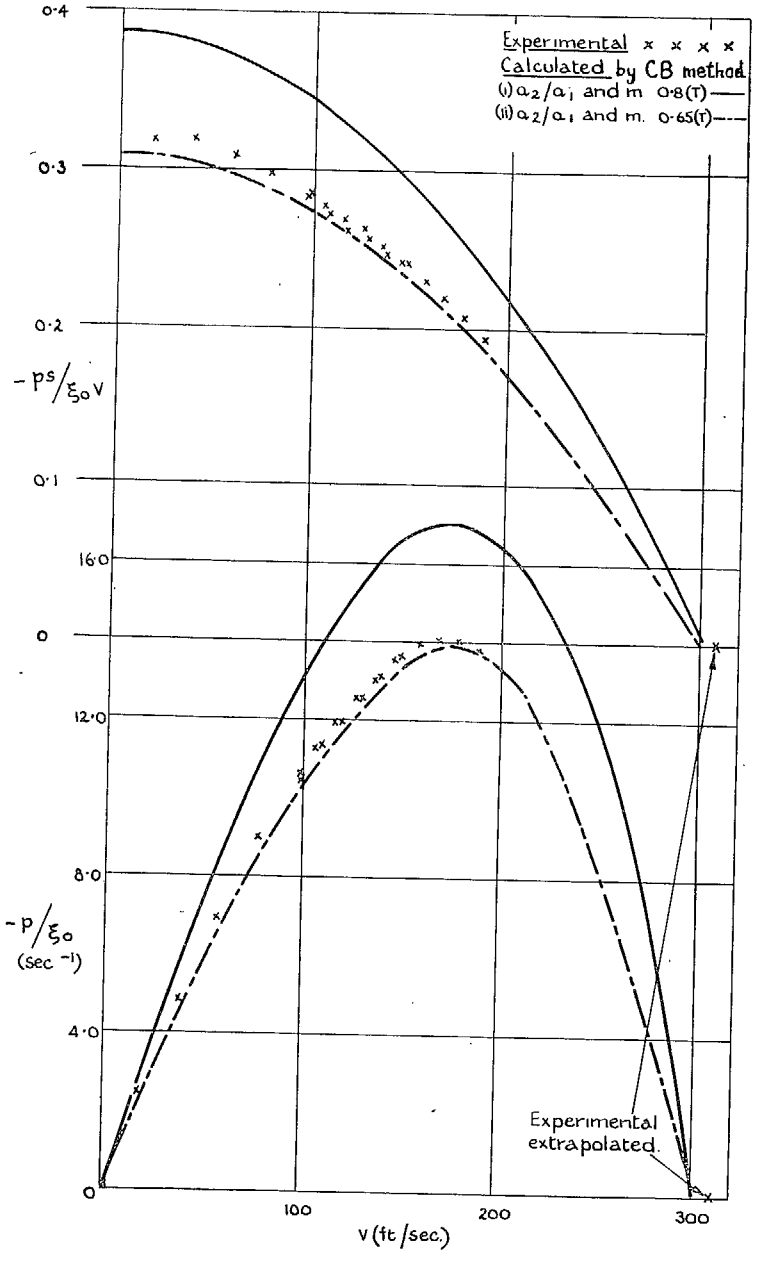

FIG. 11. Variation of rolling power with air speed.

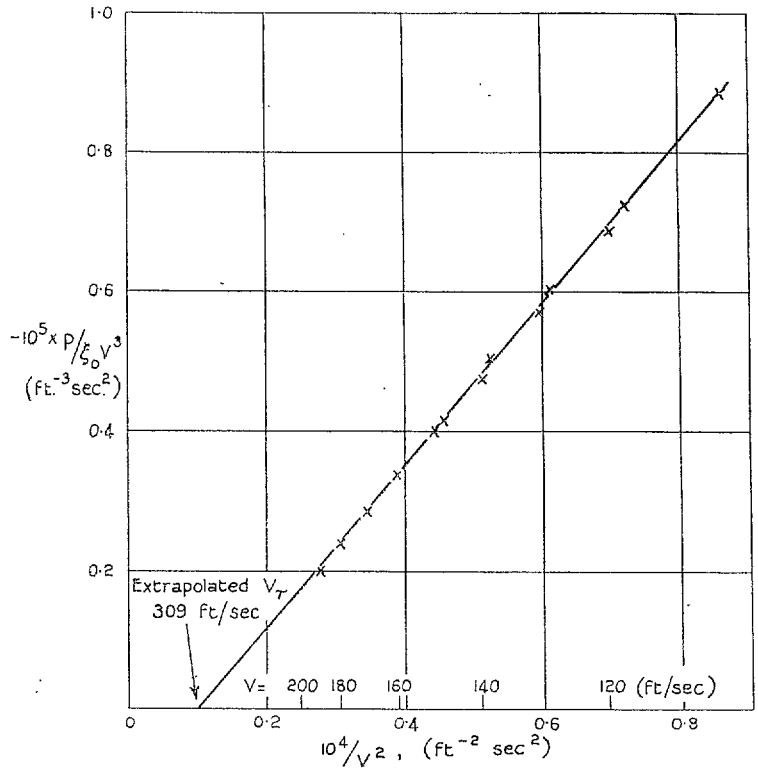

FIG. 12. Reversal speed extrapolation.

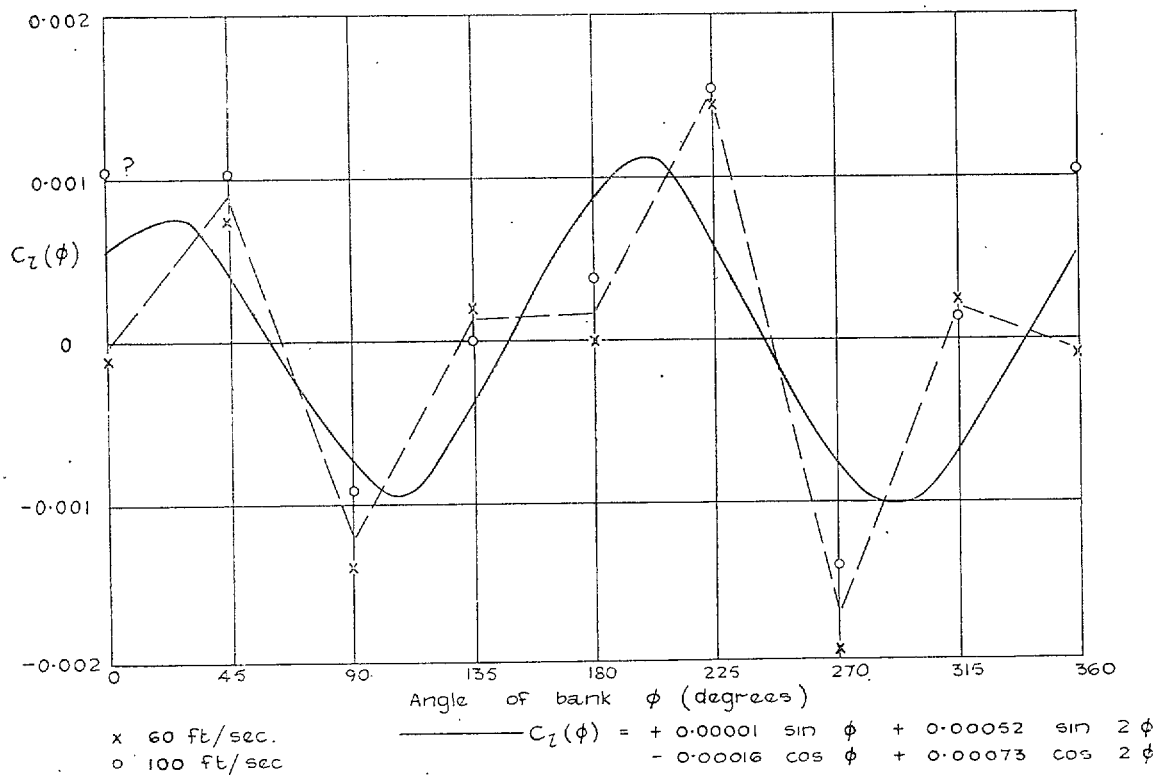

FIG. 13. Variation of rolling moment with position.

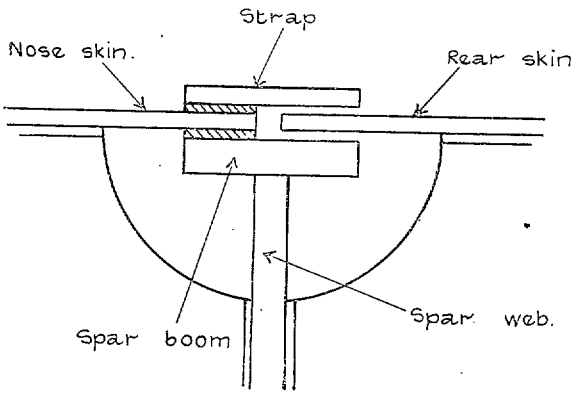

FIG. 14. The modified method of attaching the rear skin.

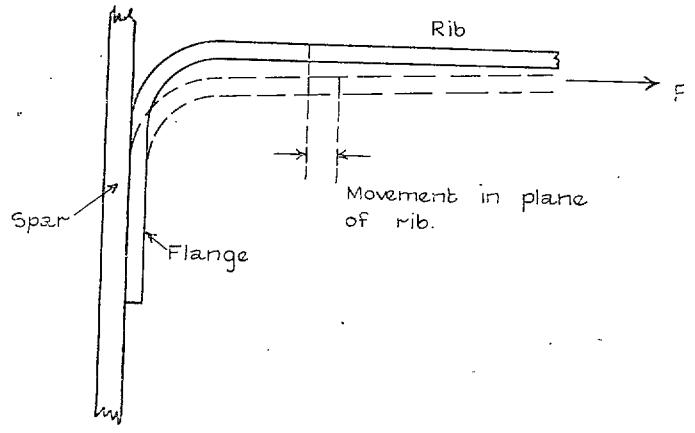

FIG. 15. Flexibility due to rib-spar joint.

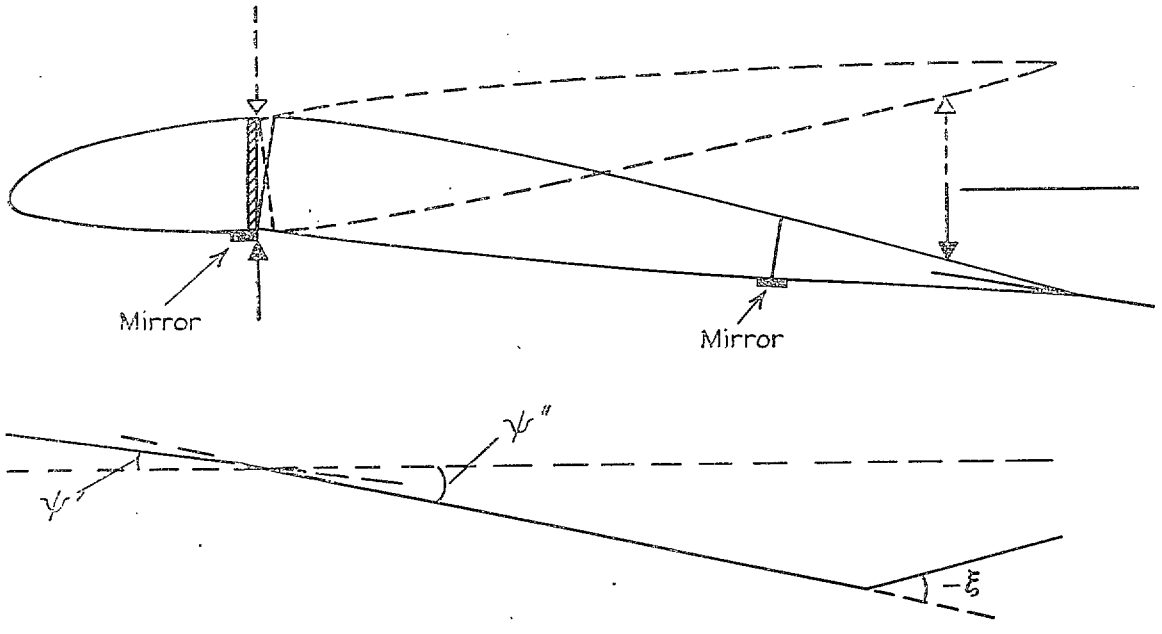

FIG. 16. Modified wings. Distortion due to a couple.

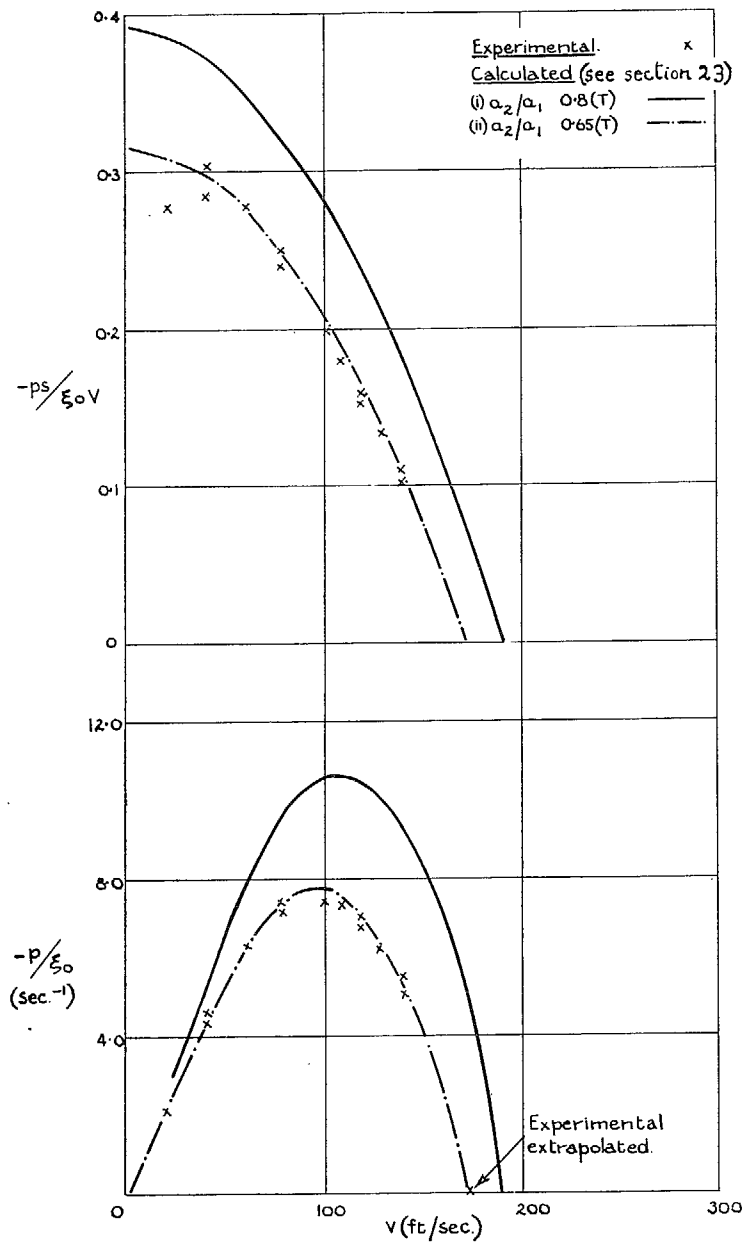

FIG. 17. Modified wings. Variation of rolling power with air speed.

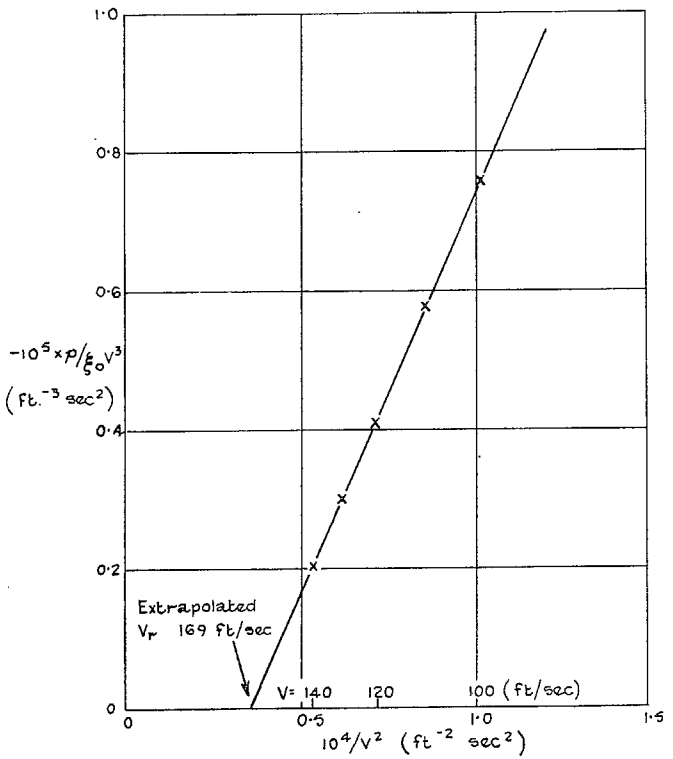

FIG. 18. Modified wing. Reversal speed extrapolation.

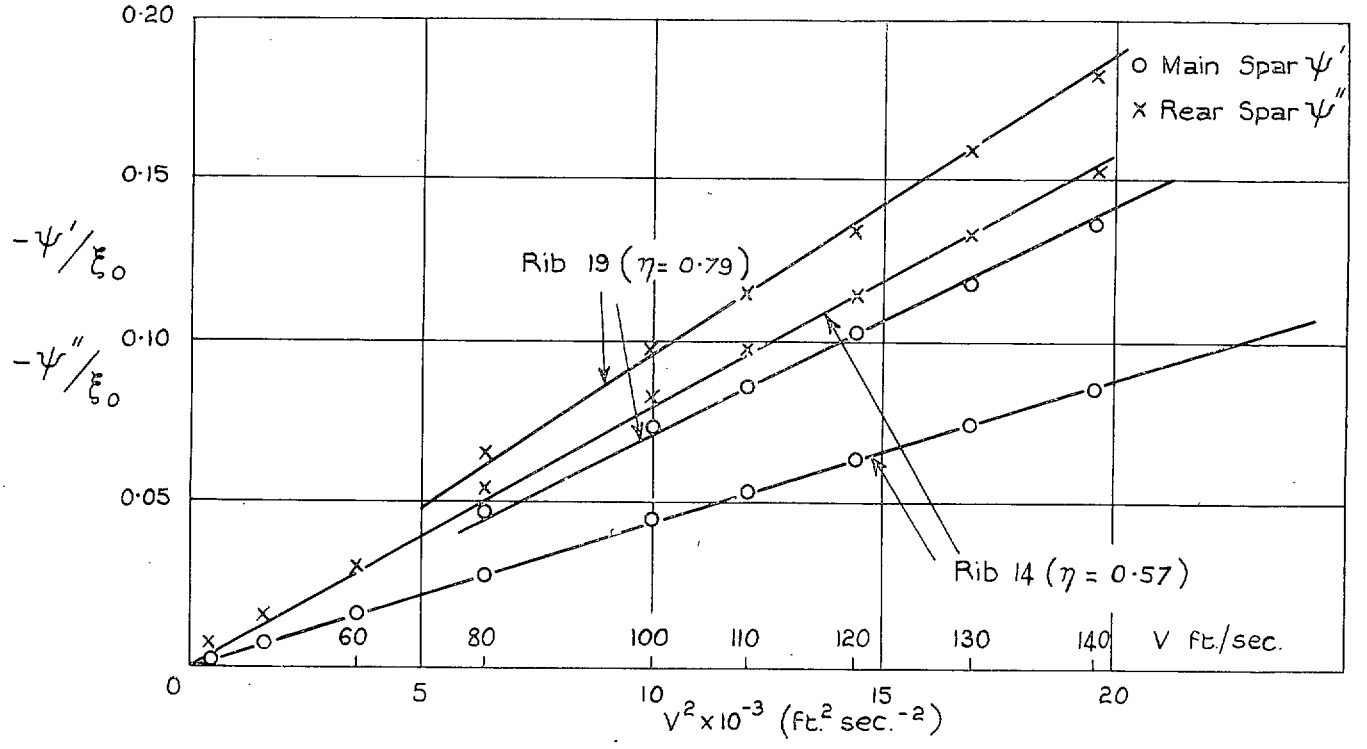

FIG. 19. Modified wings. Angular distortions during rolling at two spanwise positions. Measured on port wing for $\xi_0 = \pm 10$ deg.

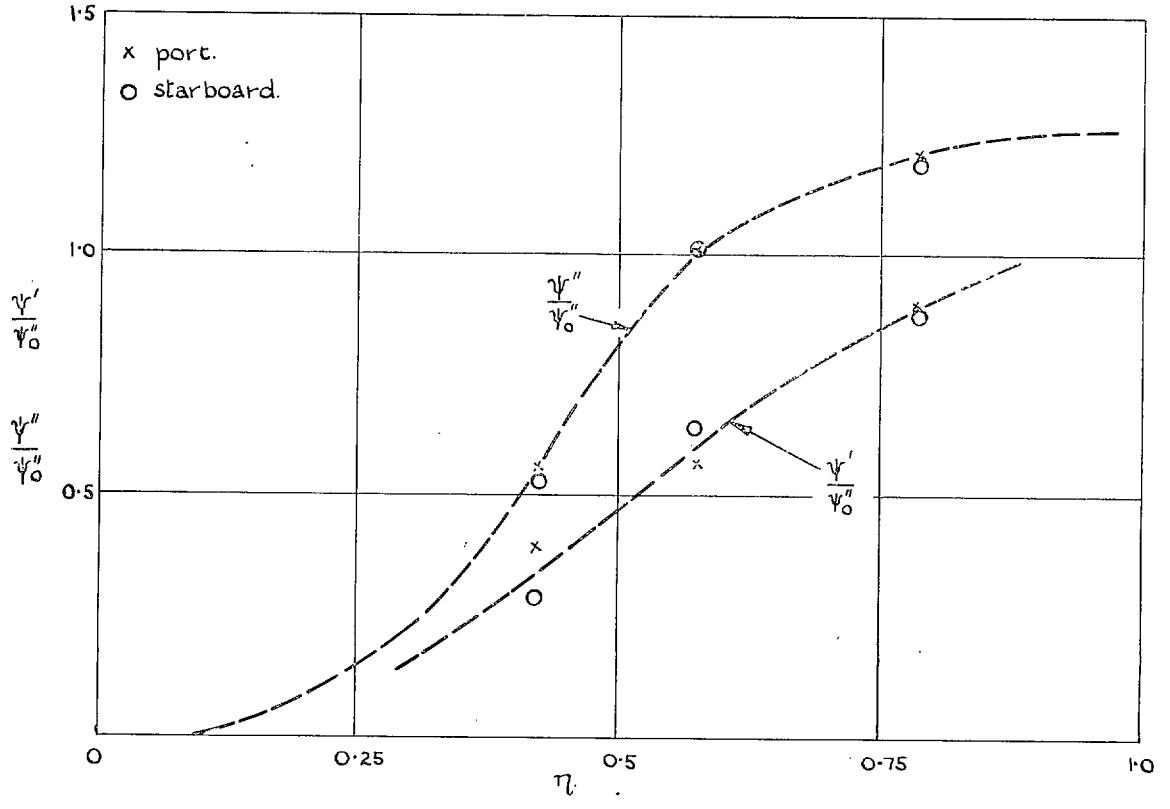

FIG. 20. Modified wings. Mode of distortion whilst rolling.

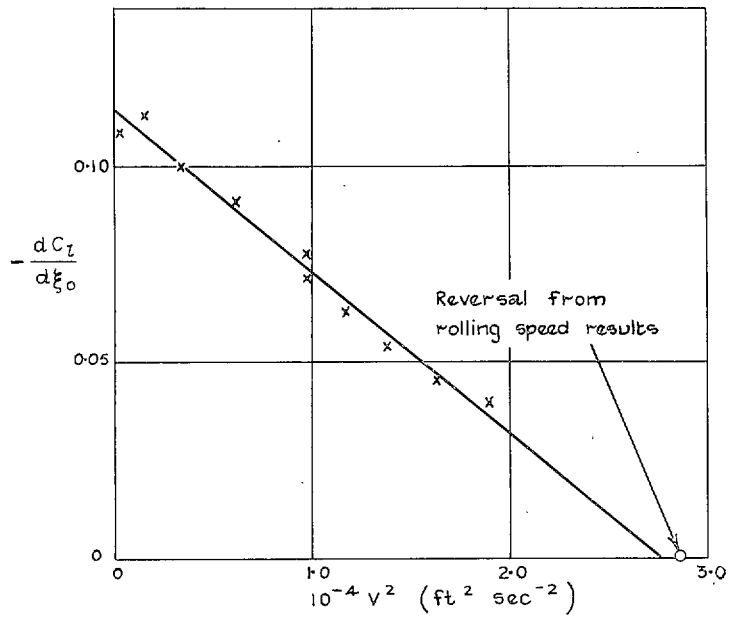

FIG. 21. Modified wings. Variation of $dC_l/d\xi_0$ with air speed.

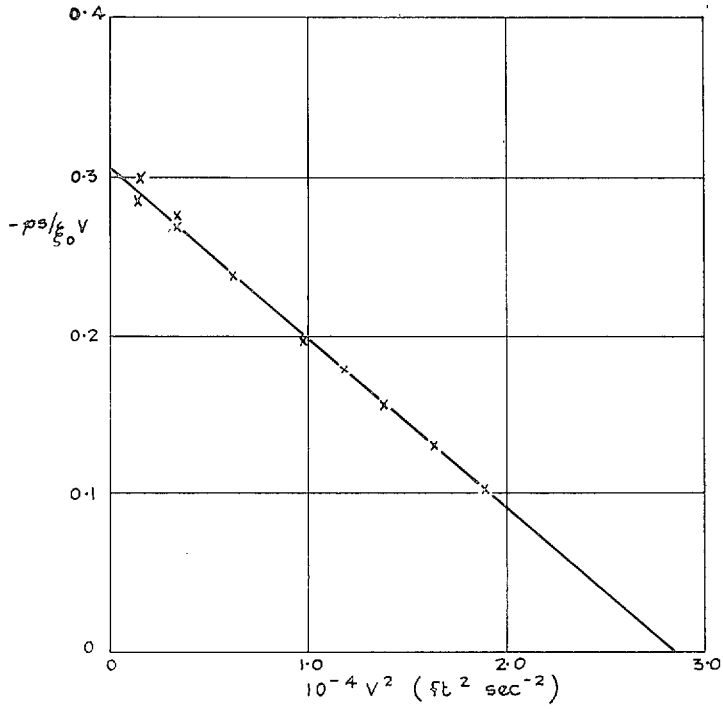

FIG. 22. Modified wings. Variation of $(ps/\xi_0 V)$ with V^2.

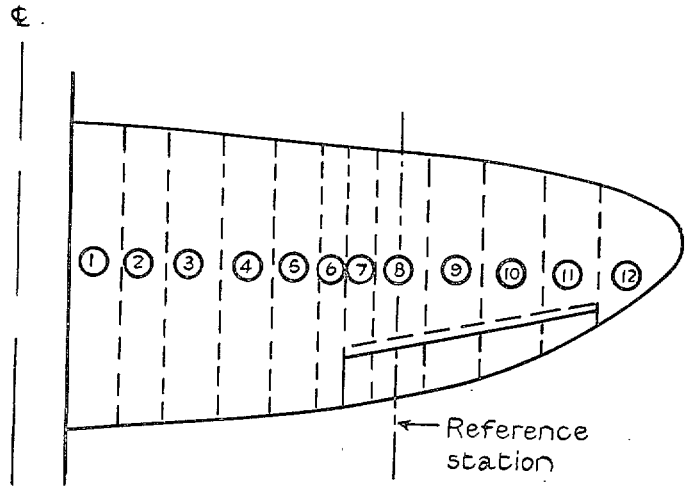

FIG. 23a. Strips used in Collar and Broadbent calculation.

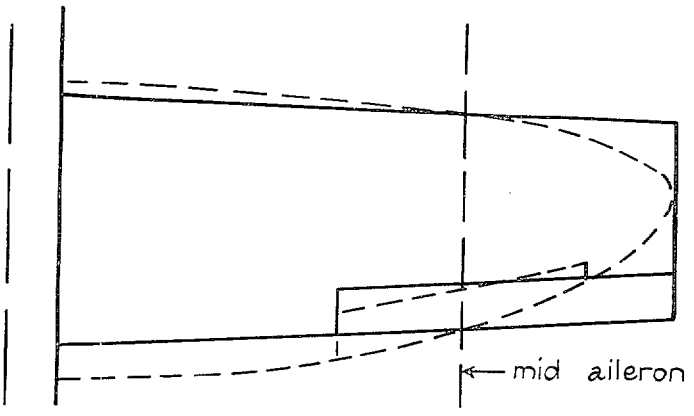

FIG. 23b. Hirst equivalent wing (complete wing).

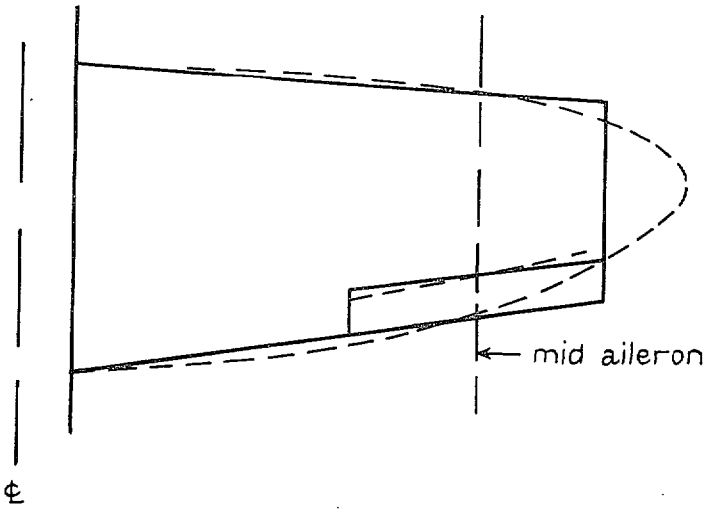

FIG. 23c. Hirst equivalent wing (wing tip neglected).

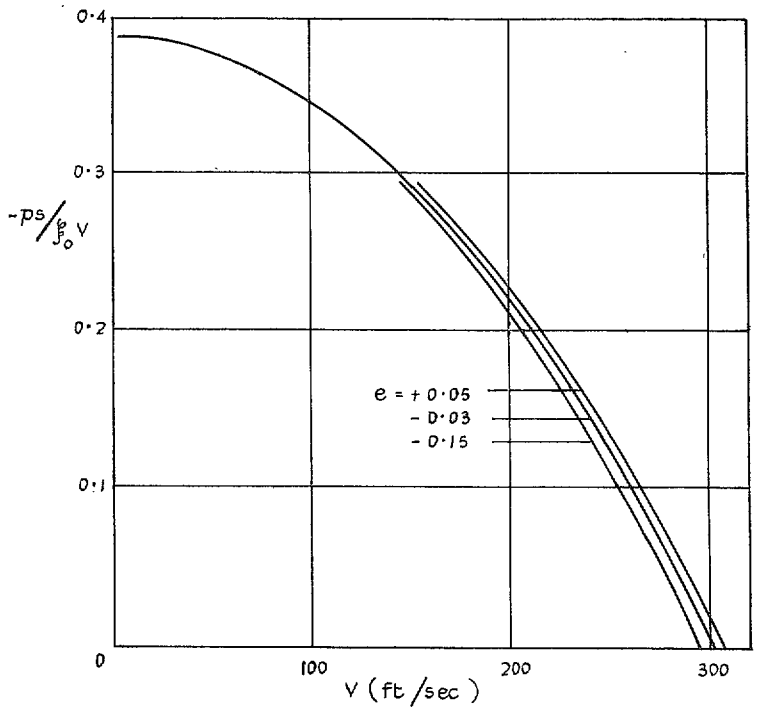

FIG. 24. Variation of rolling power with air speed. Calculated by Collar and Broadbent method for 3 positions of flexural axis.

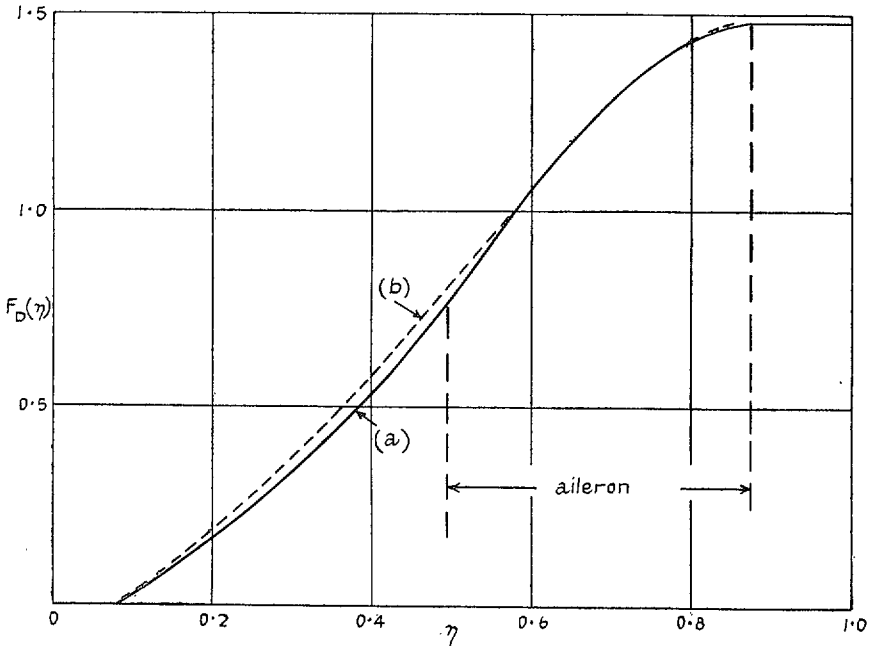

FIG. 25. Mode of twist during rolling. Calculated by : (*a*) Collar and Broadbent method, (*b*) Garner lifting-line method, referred to $\eta = 0 \cdot 575$.

J4336 19/8411 K7 10/55 D&Co. 34/263

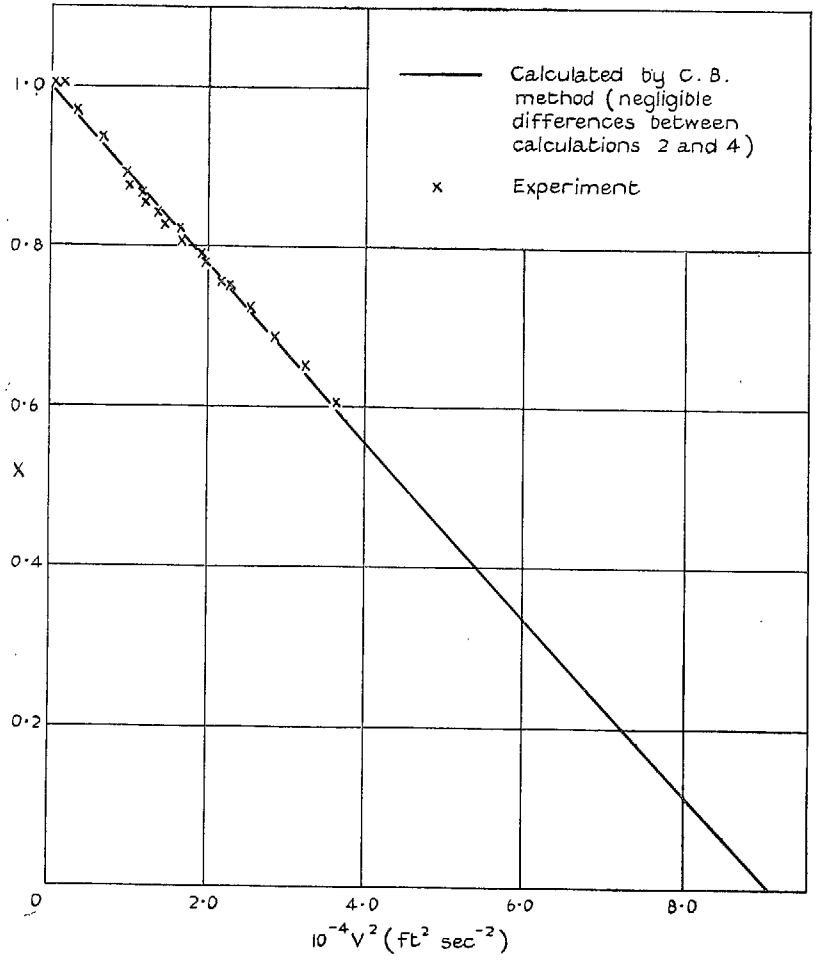

FIG. 26. Ratio (rolling power at speed V)/(' rigid-wing ' rolling power).

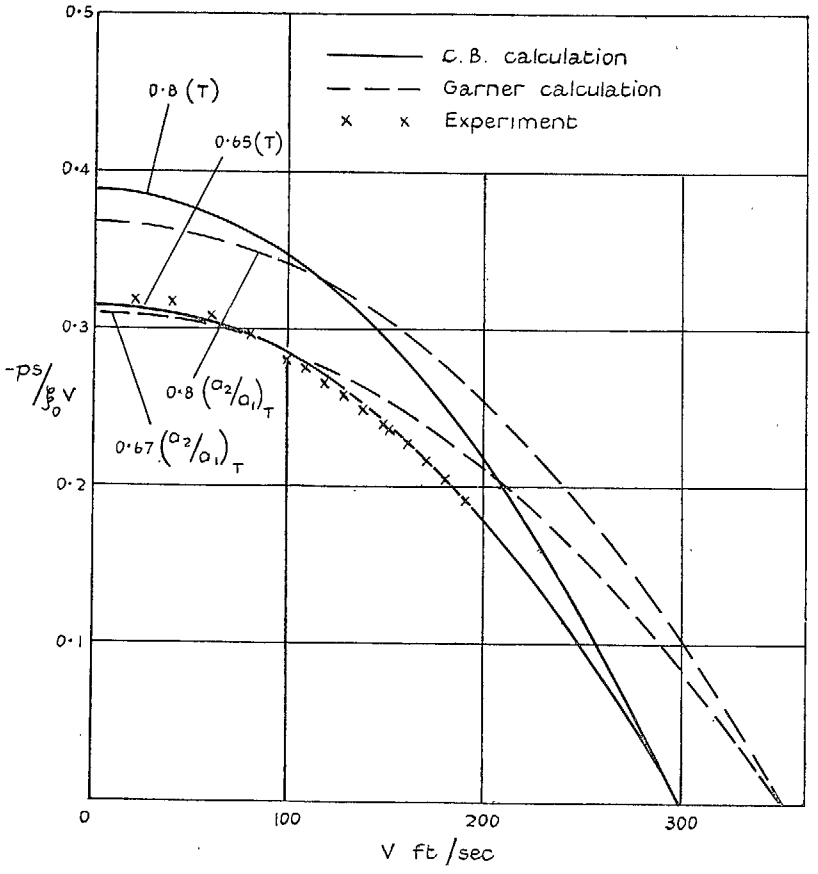

FIG. 27. Variation of rolling power with air speed.

PRINTED IN GREAT BRITAIN

Publications of the Aeronautical Research Council

ANNUAL TECHNICAL REPORTS OF THE AERONAUTICAL RESEARCH COUNCIL (BOUND VOLUMES)

1938 Vol. I. Aerodynamics General, Performance, Airscrews. 50*s*. (51*s*. 2*d*.)
Vol. II. Stability and Control, Flutter, Structures, Seaplanes, Wind Tunnels, Materials. 30*s*. (31*s*. 2*d*.)

1939 Vol. I. Aerodynamics General, Performance, Airscrews, Engines. 50*s*. (51*s*. 2*d*.)
Vol. II. Stability and Control, Flutter and Vibration, Instruments, Structures, Seaplanes, etc. 63*s*. (64*s*. 2*d*.)

1940 Aero and Hydrodynamics, Aerofoils, Airscrews, Engines, Flutter, Icing, Stability and Control, Structures, and a miscellaneous section. 50*s*. (51*s*. 2*d*.)

1941 Aero and Hydrodynamics, Aerofoils, Airscrews, Engines, Flutter, Stability and Control, Structures. 63*s*. (64*s*. 2*d*.)

1942 Vol. I. Aero and Hydrodynamics, Aerofoils, Airscrews, Engines. 75*s*. (76*s*. 3*d*.)
Vol. II. Noise, Parachutes, Stability and Control, Structures, Vibration, Wind Tunnels. 47*s*. 6*d*. (48*s*. 8*d*.)

1943 Vol. I. Aerodynamics, Aerofoils, Airscrews. 80*s*. (81*s*. 4*d*.)
Vol. II. Engines, Flutter, Materials, Parachutes, Performance, Stability and Control, Structures. 90*s*. (91*s*. 6*d*.)

1944 Vol. I. Aero and Hydrodynamics, Aerofoils, Aircraft, Airscrews, Controls. 84*s*. (85*s*. 8*d*.)
Vol. II. Flutter and Vibration, Materials, Miscellaneous, Navigation, Parachutes, Performance, Plates and Panels, Stability, Structures, Test Equipment, Wind Tunnels. 84*s*. (85*s*. 8*d*.)

ANNUAL REPORTS OF THE AERONAUTICAL RESEARCH COUNCIL—

1933–34	1*s*. 6*d*. (1*s*. 8*d*.)	1937	2*s*. (2*s*. 2*d*.)
1934–35	1*s*. 6*d*. (1*s*. 8*d*.)	1938	1*s*. 6*d*. (1*s*. 8*d*.)
April 1, 1935 to Dec. 31, 1936	4*s*. (4*s*. 4*d*.)	1939–48	3*s*. (3*s*. 2*d*.)

INDEX TO ALL REPORTS AND MEMORANDA PUBLISHED IN THE ANNUAL TECHNICAL REPORTS, AND SEPARATELY—

April, 1950 – – – – – R. & M. No. 2600. 2*s*. 6*d*. (2*s*. 7½*d*.)

AUTHOR INDEX TO ALL REPORTS AND MEMORANDA OF THE AERONAUTICAL RESEARCH COUNCIL—

1909–January, 1954 – – – R. & M. No. 2570. 15*s*. (15*s*. 4*d*.)

INDEXES TO THE TECHNICAL REPORTS OF THE AERONAUTICAL RESEARCH COUNCIL—

December 1, 1936 — June 30, 1939.	R. & M. No. 1850.	1*s*. 3*d*. (1*s*. 4½*d*.)
July 1, 1939 — June 30, 1945. –	R. & M. No. 1950.	1*s*. (1*s*. 1½*d*.)
July 1, 1945 — June 30, 1946. –	R. & M. No. 2050.	1*s*. (1*s*. 1½*d*.)
July 1, 1946 — December 31, 1946.	R. & M. No. 2150.	1*s*. 3*d*. (1*s*. 4½*d*.)
January 1, 1947 — June 30, 1947. –	R. & M. No. 2250.	1*s*. 3*d*. (1*s*. 4½*d*.)

PUBLISHED REPORTS AND MEMORANDA OF THE AERONAUTICAL RESEARCH COUNCIL—

Between Nos. 2251–2349. – –	R. & M. No. 2350.	1*s*. 9*d*. (1*s*. 10½*d*.)
Between Nos. 2351–2449. – –	R. & M. No. 2450.	2*s*. (2*s*. 1½*d*.)
Between Nos. 2451–2549. – –	R. & M. No. 2550.	2*s*. 6*d*. (2*s*. 7½*d*.)
Between Nos. 2551–2649. – –	R. & M. No. 2650.	2*s*. 6*d*. (2*s*. 7½*d*.)

Prices in brackets include postage

HER MAJESTY'S STATIONERY OFFICE

York House, Kingsway, London W.C.2; 423 Oxford Street, London W.1 (Post Orders: P.O. Box 569, London S.E.1); 13a Castle Street, Edinburgh 2; 39 King Street, Manchester 2; 2 Edmund Street, Birmingham 3; 109 St. Mary Street, Cardiff; Tower Lane, Bristol 1; 80 Chichester Street, Belfast, *or through any bookseller*

S.O. Code No. 23-2895